Charge Transport in Organic Semiconductors

Veaceslav Coropceanu,[†] Jérôme Cornil,[‡,†] Demetrio A. da Silva Filho,[†] Yoann Olivier,[‡] Robert Silbey,[#] and Jean-Luc Brédas*,[†,‡]

School of Chemistry and Biochemistry and Center for Organic Photonics and Electronics, Georgia Institute of Technology, Atlanta, Georgia 30332-0400, Laboratory for Chemistry of Novel Materials, University of Mons-Hainaut, Place du Parc 20, B-7000 Mons, Belgium, and Department of Chemistry, Massachusetts Institute of Technology, Cambridge, Massachusetts 02139-4307

Contents

1. Introduction

As exemplified by this special issue of *Chemical Reviews*, organic electronics has emerged as a vibrant field of research

and development, spanning chemistry, physics, materials science, engineering, and technology. The rapid growth in the interest given to π-conjugated materials in general and organic semiconductors in particular is fueled by both academia and industry. On the basic research side, π-conjugated materials are fascinating systems in which a rich variety of new concepts have been uncovered due the interplay between their π-electronic structure and their geometric structure.[1–3] On the applied research side, while not destined to replace silicon-based technologies, organic semiconductors promise the advent of fully flexible devices for large-area displays, solid-state lighting, radio frequency identification tags, or solar cells; major chemical companies worldwide, such as Sumitomo, DuPont, Solvay, BASF, Ciba, and Merck to name but a few, are now involved in developing efficient sources of chemicals for organic electronics applications.

The devices mentioned above share a common trait: in all instances, their performance critically depends on the efficiency with which charge carriers (electrons and/or holes) move within the π-conjugated materials. The charge carriers are either injected into the organic semiconductors from metal or conducting oxide electrodes in the case of light-emitting diodes or field-effect transistors or generated within the materials in the case of solar cells via photon-induced charge separation at the interface between electron-donor and electron-acceptor components.

In an earlier *Chemical Reviews* article,[4] we discussed how the various energy-transfer and charge-transfer processes that take place in π-conjugated polymers and oligomers can now be described at the molecular level. Here, we focus on charge transport in these organic materials. In section 2, we briefly describe the main experimental techniques used to evaluate carrier mobilities. We then introduce the organic materials that have been the subject of most investigations and discuss the factors that directly affect the mobilities. Section 3 deals with a detailed description of the charge-transport parameters: electronic couplings, site energies, and electron–phonon couplings. In section 4, we present an overview of the models that have been reported to describe the charge-transport mechanisms in molecular crystals and disordered organic materials. A brief synopsis is given in section 5.

2. Characterization of Charge Mobility

Organic semiconductors can be broadly classified into two categories: small molecules or oligomers (usually processed in vacuum) and polymers (usually processed by wet chemical techniques). In each case, various materials have been designed over the years that preferentially transport holes or electrons. In most instances, this distinction does not rely

* To whom correspondence should be addressed.
† Georgia Institute of Technology.
‡ University of Mons-Hainaut.
# Massachusetts Institute of Technology.

Veaceslav Coropceanu received his Ph.D. in Theoretical and Mathematical Physics from the State University of Moldova in 1985. In 1994, he was appointed as Associate Professor at the same university. After research stays at the University of Sussex, United Kingdom, on a NATO/Royal Society Fellowship and at the Medical University of Lübeck, Germany, on an Alexander von Humboldt Fellowship, he joined the Brédas research group in 2000. He is currently a Senior Research Scientist at the Georgia Institute of Technology. His present research interests include the investigation of the electronic properties of organic and inorganic systems, electron-transfer phenomena, and the theory of vibronic coupling.

Demetrio Filho was born in Pernambuco (Brazil) in 1974. In 2003, he received his Ph.D. in Physics from the State University of Campinas in São Paulo (Brazil) under the supervision of Prof. Maria Cristina dos Santos. During his Ph.D., he was awarded a scholarship to spend one year in the group of Prof. Jean-Luc Brédas, then at the University of Arizona. After completing his Ph.D., he returned to Prof. Brédas' group for a postdoctoral stay. He is currently a Research Scientist at the Georgia Institute of Technology. His research interests include the theoretical investigation of novel organic semiconductors with particular focus on charge transport.

Jérôme Cornil was born in Charleroi, Belgium, in 1970. He received his Ph.D. in Chemistry from the University of Mons-Hainaut in 1996 and then went for a postdoctoral stay at UCSB (with Alan Heeger) and MIT (with Bob Silbey). He is a Research Associate of the Belgian National Fund for Scientific Research (FNRS) in Mons and since 2005 holds a Visiting Principal Research Scientist position at the Georgia Institute of Technology. His main research interests deal with the quantum-chemical characterization of the electronic and optical properties of organic conjugated materials, in relation to their use in opto-electronic devices.

Yoann Olivier was born in La Louvière, Belgium, in 1982. He graduated with a B.S. in Physics from the University of Mons-Hainaut in 2004 and is presently a Ph.D. student in the Laboratory for Chemistry of Novel Materials. His research focuses on the theoretical characterization of charge transport in molecular crystals and disordered systems.

on the actual ability of the materials to transport charges (i.e., on the actual values of charge mobilities) but rather reflects the ease of charge injection from electrodes traditionally used in devices. In that context, a material is often referred to as a hole [electron] transporter when its ionization energy [electron affinity] closely matches the Fermi level of the electrode material. Ambipolar transport (i.e., the ability to transport both electrons and holes) has now been reported for several organic semiconductors and is discussed in this issue by Sirringhaus and Zaumseil.[5]

The key quantity that characterizes charge transport is the carrier mobility. In the absence of any external potential, transport is purely diffusive and is generally described by a simple diffusion equation:

$$\langle x^2 \rangle = nDt \qquad (1)$$

where $\langle x^2 \rangle$ denotes the mean-square displacement of the charges, D is the diffusion coefficient, t is the time, and n represents an integer number equal to 2, 4, or 6 for one-, two-, and three-dimensional (1D, 2D, and 3D) systems, respectively. The charge mobility μ is related to the diffusion coefficient via the Einstein−Smoluchowski equation:

$$\mu = \frac{eD}{k_B T} \qquad (2)$$

where k_B is the Boltzmann constant and e is the electron charge.

The application of an external electric field induces a drift of the charge carriers; the mobility can then be alternatively defined as the ratio between the velocity, v, of the charges and the amplitude of the applied electric field, F:

$$\mu = v/F \qquad (3)$$

Diffusion should be seen as a local displacement of the

Robert Silbey was born in Brooklyn, New York, and graduated from Brooklyn College in 1961. He received his Ph.D. in Chemistry from the University of Chicago in 1965 and then held a postdoctoral appointment at the University of Wisconsin, working with the late Joseph Hirschfelder. He has been on the faculty of MIT since 1966 and at present is the Class of '42 Professor of Chemistry and Dean of Science. He was elected to the National Academy of Sciences in 2003. His main research interests deal with the theoretical studies of electronic and optical properties of polymers, relaxation and coherence in low temperature systems, and the spectroscopy of molecules in condensed phase, in particular, single molecule and hole burning spectroscopy.

Jean-Luc Brédas received his Ph.D. in Chemistry in 1979 from the University of Namur, Belgium, under the supervision of Jean-Marie André. For his postdoctoral stay in 1980–1981, he joined Bob Silbey at MIT and Ron Chance at the (then) Allied Chemical Corporate Research Center in Morristown, New Jersey, to work on a joint university–industry NSF project on conducting polymers. After his postdoc, he went back to Namur as a Research Fellow of the Belgian National Science Foundation. In 1988, he was appointed Professor at the University of Mons-Hainaut, Belgium, where he established the Laboratory for Chemistry of Novel Materials. While keeping an "Extraordinary Professorship" appointment in Mons, Jean-Luc Brédas joined the University of Arizona in 1999 before moving in 2003 to the Georgia Institute of Technology. At Georgia Tech, he is Professor of Chemistry and Biochemistry and the Georgia Research Alliance Eminent Scholar and Chair in Molecular Design. Since 2001, he has been a member of the European Union Research Advisory Board (EURAB) for Science, Technology, and Innovation. The research interests of his group focus on the computational design of novel organic materials with remarkable electrical and optical properties.

charge around an average position, while drift induces a displacement of the average position. Drift is the effect that dominates the migration of the charges across an organic layer in the devices. The carrier mobility is usually expressed in $cm^2/V \cdot s$ (since it corresponds to velocity over electric field).

2.1. Experimental Measurements of Carrier Mobilities

Charge mobilities can be determined experimentally by various techniques.[6] Results from methods that measure mobilities over macroscopic distances ($\sim$1 mm) are often dependent on the purity and order in the material. Methods that measure mobilities over microscopic distances are less dependent on these characteristics. We briefly describe below the basic principles of some of the most widely referenced methods.

2.1.1. Time-of-Flight (TOF)

Here, an organic layer a few microns thick is sandwiched between two electrodes. The material is first irradiated by a laser pulse in the proximity of one electrode to generate charges. Depending on the polarity of the applied bias and the corresponding electric field (in the 10^4–10^6 V/cm range), the photogenerated holes or electrons migrate across the material toward the second electrode. The current at that electrode is recorded as a function of time. A sharp signal is obtained in the case of ordered materials while in disordered systems a broadening of the signal occurs due to a distribution of transient times across the material. The mobility of the holes or electrons is estimated via:

$$\mu = \frac{v}{F} = \frac{d}{Ft} = \frac{d^2}{Vt} \tag{4}$$

where d is the distance between the electrodes, F is the electric field, t is the averaged transient time, and V is the applied voltage. TOF measurements clearly show the impact on mobility of structural defects present in the material. Charge mobilities in organic materials were first measured with the TOF technique by Kepler[7] and Leblanc.[8]

2.1.2. Field-Effect Transistor Configuration

The carrier mobilities can be extracted from the electrical characteristics measured in a field-effect transistor (FET) configuration. As reviewed by Horowitz,[9] the I–V (current–voltage) expressions derived for inorganic-based transistors in the linear and saturated regimes prove to be readily applicable to organic transistors (OFETs). These expressions read in the linear regime:

$$I_{SD} = \frac{W}{L}\mu C(V_G - V_T)V_{SD} \tag{5}$$

and in the saturated regime:

$$I_{SD} = \frac{W}{2L}\mu C(V_G - V_T)^2 \tag{6}$$

Here, I_{SD} and V_{SD} are the current and voltage bias between source and drain, respectively, V_G denotes the gate voltage, V_T is the threshold voltage at which the current starts to rise, C is the capacitance of the gate dielectric, and W and L are the width and length of the conducting channel. In FETs, the charges migrate within a very narrow channel (at most a few nanometers wide) at the interface between the organic semiconductor and the dielectric.[10,11] Transport is affected by structural defects within the organic layer at the interface, the surface topology and polarity of the dielectric, and/or the presence of traps at the interface (that depends on the chemical structure of the gate dielectric surface). Also,

contact resistance at the source and drain metal/organic interfaces plays an important role; the contact resistance becomes increasingly important when the length of the channel is reduced and the transistor operates at low fields; its effect can be accounted for via four-probe measurements.[12−14]

The charge mobilities extracted from the OFET $I-V$ curves are generally higher in the saturated regime than those in the linear regime as a result of different electric-field distributions. The mobility can sometimes be found to be gate-voltage dependent;[15] this observation is often related to the presence of traps due to structural defects and/or impurities (that the charges injected first have to fill prior to establishment of a current) and/or to dependence of the mobility on charge carrier density (which is modulated by V_G).[16]

The dielectric constant of the gate insulator also affects the mobility; for example, measurements on rubrene single crystals[17] and polytriarylamine chains[18] have shown that the carrier mobility decreases with increasing dielectric constant due to polarization (electrostatic) effects across the interface; the polarization induced at the dielectric surface by the charge carriers within the organic semiconductor conducting channel, couples to the carrier motion, which can then be cast in the form of a Frölich polaron.[19−22]

2.1.3. Diode Configuration

The mobilities can also be obtained from the electrical characteristics of diodes built by sandwiching an organic layer between two electrodes (provided that transport is bulk limited and not contact limited). The choice of the electrodes is generally made in such a way that only electrons or holes are injected at low voltage. In the absence of traps and at low electric fields, the current density J scales quadratically with applied bias V. Such behavior is characteristic of a space-charge limited current (SCLC); it corresponds to the current obtained when the number of injected charges reaches a maximum because their electrostatic potential prevents the injection of additional charges.[23] In that instance, the charge density is not uniform across the material and is largest close to the injecting electrode.[24] In this regime, when neglecting diffusion contributions, the $J-V$ characteristics can be expressed as

$$J = \frac{9}{8}\epsilon_0\epsilon_r\mu\frac{V^2}{L^3} \tag{7}$$

where ϵ_r denotes the dielectric constant of the medium and L is the device thickness. Note that a field-dependence of the mobility has to be considered at high electric fields (vide infra).

The $J-V$ curves become more complex in the presence of traps. They first exhibit a linear regime, where transport is injection-limited, followed by a sudden increase for an intermediate range of applied biases; finally, the V^2 dependence of the trap-free SCLC regime is reached. The extent of the intermediate region is governed by the spatial and energetic distribution of trap states,[14] which is generally modeled by a Gaussian[25] or exponential distribution.[26]

2.1.4. Pulse-Radiolysis Time-Resolved Microwave Conductivity (PR-TRMC)

Here, the sample is first excited by a pulse of highly energetic electrons (in the MeV range) to create a low density of free carriers. The change in electrical conductivity $\Delta\sigma$ induced by the pulse is then measured via the change in microwave power reflected by the sample and is therefore frequency dependent. $\Delta\sigma$ can be expressed as[27]

$$\Delta\sigma = e\sum\mu N_{e-h} \tag{8}$$

where $\sum\mu$ is the sum of hole and electron mobilities and N_{e-h} is the density of generated electron−hole pairs. N_{e-h} is estimated by dividing the amount of energy density transferred to the material by the energy required to create one electron−hole pair; this ratio is further multiplied by a survival probability that accounts for possible charge-recombination mechanisms during the duration of the pulse. With this technique, the charges are directly generated in the bulk; their transport properties are probed on a very local spatial scale (for instance, along a portion of a single polymer chain) determined by the frequency of the microwave radiations (the lower the frequency, the larger the region that is explored); the charges trapped by impurities or structural defects are not responsive. PR-TRMC is a contact-free technique that is not affected by space-charge effects and can be applied to bulk materials as well as to single polymer chains in solution.

Because of its local character, PR-TRMC is considered to provide intrinsic AC mobility values for the bulk; these values should be seen as upper limits for the mobilities at low fields. TOF values are generally smaller since such DC measurements probe a macroscopic range and force the charge carriers to cross structural defects and to interact with impurities. The AC and DC mobility values generally deviate above a threshold frequency that depends on the degree of order in the samples. However, there are instances in which the two techniques result in similar mobility values, for example, in the case of discotic liquid crystals based on hexathiohexyl triphenylenes, materials that have been used as reference compounds to validate the PR-TRMC technique.[28] PR-TRMC experiments on polythienylenevinylene[29] and polyparaphenylenevinylene[30] chains provide hole [electron] mobility values of 0.38 [0.23] and 0.06 [0.15] cm²/V·s, respectively (here, one kind of charge carriers was alternatively selectively trapped to determine the individual mobilities). A mobility as high as 600 cm²/V·s has been recently inferred from measurements in dilute solution along fully planar, ladder-type polyparaphenylene chains;[31] this result confirms that the elimination of torsional degrees of freedom along polymer chains is a key step to increase charge mobilities. In polymer films, charge mobilities are expected to be limited by interchain transport; to reach mobilities over 0.1 cm²/V·s requires a high degree of interchain structural order.

2.2. Materials

Charge transport in *molecular* materials has received much attention since a number of conjugated molecules can be grown in the form of reasonably large single crystals by vacuum sublimation techniques under controlled conditions. Well-defined structures with a limited number of impurities can be obtained through repeated sublimation steps.[32] Such crystals provide an ideal test bed to investigate the fundamental parameters affecting charge mobilities. However, their slow growth and lack of processability prevent them from being integrated in industrial processes. For industrial applications, cost-effective approaches are sought after, based in particular on solution processing of (substituted) molecules
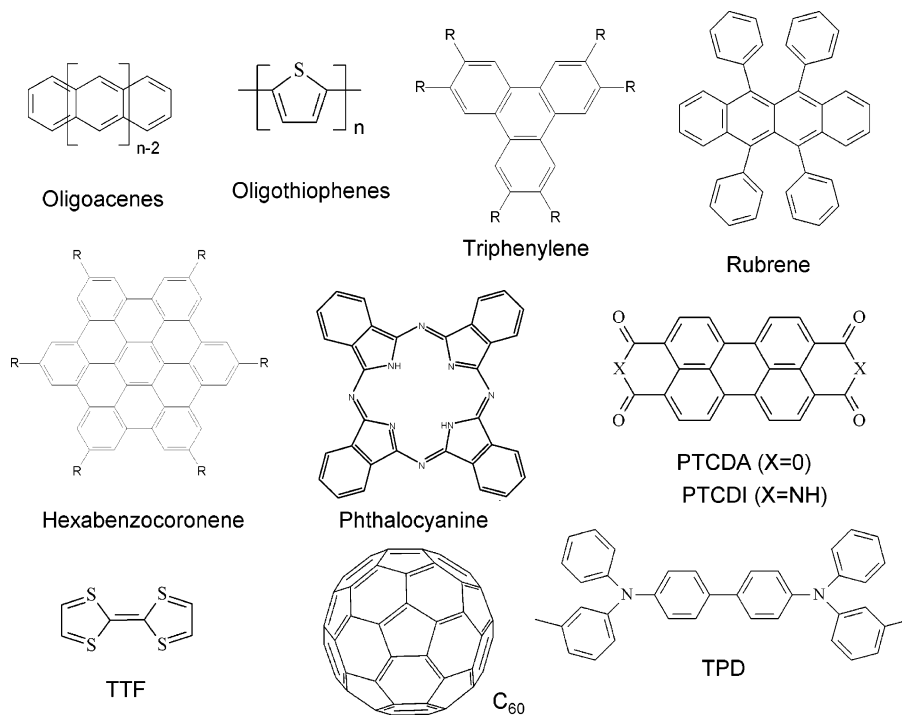
Figure 1. Chemical structures of some of the most studied organic molecular semiconductors (see text for detail).

or on the deposition of polycrystalline or amorphous films by vacuum sublimation. In the best cases, the room-temperature mobility of crystalline organic semiconductors can reach the 0.1−20 cm²/V·s range;[6,33,34] in amorphous materials, the mobility generally drops well below 0.1 cm²/V·s.[35,36]

Some of the most widely investigated molecular semiconductors are illustrated in Figure 1. They belong to the families of the following.

Oligoacenes.[32,37] This class of materials, which has been studied for several decades,[38] currently provides among the best semiconductors in the field of organic electronics. Special attention has been given to pentacene ($n = 5$), tetracene ($n = 4$), and derivatives, which have well-defined crystal structures.[39] Among the derivatives, rubrene (a tetracene molecule substituted by four phenyl rings) has been the focus of many recent studies.[14,34,40−42] Pentacene exhibits several crystal polymorphs, which has proven useful to investigate crystal structure-transport relationships.[43]

Oligothiophenes.[44−46] The crystal structures of oligothiophenes are available for the $n = 2, 3, 4, 5, 6$, and 8 oligomers and a number of substituted derivatives. The interest in this class of materials has been intense ever since the first organic transistor, built with sexithienyl ($n = 6$) as the active semiconducting material, was reported.[47] While most oligothiophene and oligoacene compounds are used as p-type materials (that is, as hole transporters), their backbone can be derivatized with fluorinated substituents to yield efficient n-type materials (electron transporters).[48−51]

Discotic Liquid Crystals.[52] These materials are based on 2D, disc-like molecules made of a central conjugated core substituted by saturated chains on the periphery. In the discotic phase, these molecules organize in the form of quasi-1D columns that provide 1D pathways for electron and/or hole transport (the n- or p-type character can be tuned as a function of the nature of the substituents). Representative systems are based on triphenylene, hexabenzocoronene, perylenediimide, or metal phthalocyanine cores. In spite of

the absence of crystalline order, mobility values on the order of 0.5 cm²/V·s have been reported in discotic phases of hexabenzocoronene derivatives;[53] a room-temperature SCLC electron mobility as high as 1.3 cm²/V·s has been even measured for a perylenediimide derivative under ambient conditions (the latter value is higher than that of amorphous silicon).[54] Transport in liquid crystals formed by rodlike molecules has also been investigated.[55,56]

Triphenylamines. These compounds, such as the prototypical 4,4′-bis(*N*-*m*-tolyl-*N*-phenylamino)biphenyl (TPD) molecule, have a long history as organic photoconductors in the Xerox industry.[57] They have been extensively used in organic light-emitting diodes as hole-transporting materials under the form of vacuum-deposited amorphous films.[35]

Perylenes, Tetrathiafulvalenes, and Fullerenes. Perylene exhibits a peculiar crystal packing in which dimers (and not single molecules) are arranged in an herringbone fashion;[58] the attachment of dianhydride (PTCDA) or diimide (PTCDI) moieties leads to compounds with good n-type properties.[12]

Tetrathiafulvalene and derivatives have been initially widely investigated as donor entities in highly conducting charge-transfer salts.[59,60] Work has now been extended to their transport properties in thin films and crystals.[61−63]

The interest in fullerene (C₆₀) and derivatives[64,65] stems from their extensive use as electron acceptors in organic blends for photovoltaics. We also note that in the case of single-wall carbon nanotubes, ballistic transport has been measured with carrier mobilities on the order of 80 000 cm²/V·s.[66] Ballistic transport implies that the carrier mean free path is longer than the nanotube.

Charge transport in conjugated polymer chains is also the focus of many investigations. For totally disordered polymer films, charge mobilities are small, in the range $10^{-6}-10^{-3}$ cm²/V·s. Mobilities significantly increase when the polymer chains present self-assembling properties that can be exploited to generate ordered structures.[67] High mobilities can also be achieved via introduction of a liquid crystal charac-
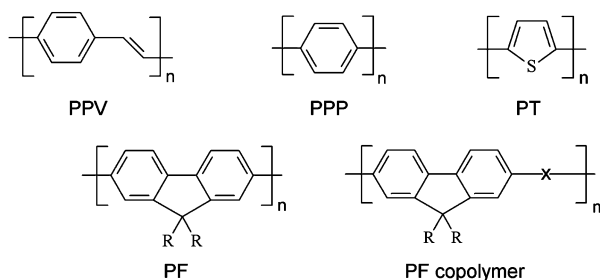
Figure 2. Chemical structures of some of the most studied organic polymeric semiconductors (see text for detail): polyparaphenylenevinylene (PPV), polyparaphenylene (PPP), polythiophene (PT), polyfluorene (PF), and polyfluorene copolymers (where X stands for various (hetero)cycles).

Figure 3. Polar plot illustrating the mobility anisotropy within the herringbone layer in a pentacene single-crystal FET (adapted from ref 79).

ter.[68,69] Among the most studied polymers, we find (see Figure 2) the following.

Polyparaphenylene, Polyparaphenylenevinylene, and Their Derivatives. These polymers were initially the focus of many experimental and theoretical studies in view of their high luminescence quantum yield in the solid state, a feature of major interest for light-emitting applications.[70,71]
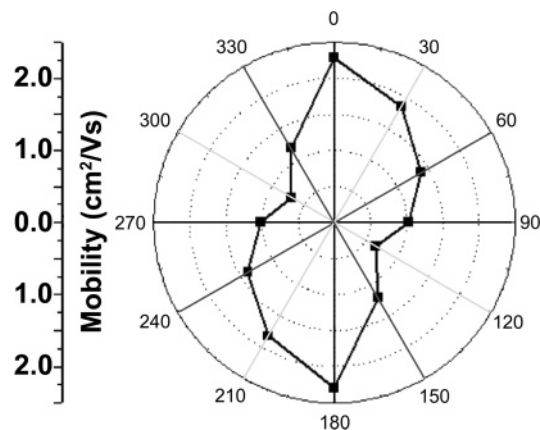
Polyfluorene (PF) and Some of Its Alternating Copolymers. These materials represent a new generation of light-emitting polymers with high purity and stability.[72]

Polythiophene (PT) and Derivatives. The regio-regular alkyl-substituted polythiophenes currently display among the highest hole mobilities (around 0.1 cm^2/V·s) due to their packing in well-organized lamellae.[67] Even higher mobilities on the order of 0.6 cm^2/V·s have been recently reported for polythiophene derivatives incorporating fused thiophene rings.[68]

π-Conjugated polymers are generally exploited as p-type materials. However, polymers with high electron affinity, such as the poly(benzobisimidazobenzophenanthrolines),[73] can be used as n-type transporters. At this stage, it is important to recall that the characterization usually found in the literature of an organic semiconductor as p-type or n-type most often *does not* reflect the intrinsic ability of the material to transport holes or electrons; it rather translates the ease with which holes or electrons can be injected into the material from the electrodes. Our experience, coming from the results of a large number of theoretical investigations over the past few years,[74,75] points to the conclusion that, in many organic semiconductors, the electron and hole mobilities are expected to be comparable. In addition, the observation of a low n-type mobility is generally the consequence of extrinsic effects, such as the presence of specific traps for electrons (due to photo-oxidation of the π-conjugated backbone) or the instability of radical-anions with respect to water, hydroxyl groups, or oxygen.[76,77] The latter has been elegantly demonstrated recently by the Cambridge group.[78] It was shown that SiO$_2$, commonly used as gate dielectric in OFETs, presents a large number of hydroxyl groups on its surface, which act as traps for electrons injected into the organic semiconductor channel. When the dielectric is covered by a tetramethylsiloxane-bis(benzocyclobutene) derivative (BCB), good n-type transport is measured for polythiophene, polyparaphenylenevinylene, and polyfluorene derivatives (mobilities in the range $10^{-2}-10^{-3}$ cm^2/V·s).[78]

2.3. Factors Influencing Charge Mobility

Efficient charge transport requires that the charges be able to move from molecule to molecule and not be trapped or scattered. Therefore, charge carrier mobilities are influenced by many factors including molecular packing, disorder, presence of impurities, temperature, electric field, charge-carrier density, size/molecular weight, and pressure. It would be too formidable a task to try to discuss all the experimental studies reported to date on the impact of these parameters on charge transport in organic semiconductors. Rather, our goal here is to focus on some selected examples, chosen to illustrate in the most simple way the role of these various factors.

2.3.1. Molecular Packing

The anisotropy of charge transport in single crystals points out that the efficiency of transport is intimately related to the relative positions of the interacting molecules, and hence to crystal packing. In most instances, unsubstituted π-conjugated molecules crystallize into a layered herringbone packing. Such packing gives rise to 2D transport within the stacked organic layers[9] while transport between layers is less efficient. The anisotropy is generally measured by orienting the crystal along the two crystal axes defining a layer. An elegant approach to build OFETs by laminating an organic crystal onto a transistor stamp has been recently reported.[41] This approach allows for multiple relamination steps with the same material and has been exploited with a rubrene single crystal to measure the mobility in multiple directions within the herringbone layer. The results indicate that the room-temperature hole mobilities along the crystallographic *a* and *b* axes (within the herringbone layer) correspond to values of 3 and 15 cm^2/V·s for the linear and saturated regimes, respectively, and the mobility ratio between the *a* and *b* directions is measured to be between 3 and 4 in the linear regime. The mobility anisotropy has also been characterized experimentally for a pentacene single crystal contacted by an electrode array;[79] the mobility within the layer is found to vary between 2.3 and 0.7 cm^2/V·s as a function of polar angle, see Figure 3.

The 2D character of transport in most organic single crystals (and thin films by extension) has implications for OFET operation since it requires the long axes of the molecules to stand perpendicular to the dielectric surface in order for a significant current to be generated within the channel. Interestingly, it was demonstrated in the case of pentacene transistors that the packing at the interface with the dielectric is different from that in the bulk.[80] We note that such variations in packing have to be properly taken into account when comparing theoretical and experimental
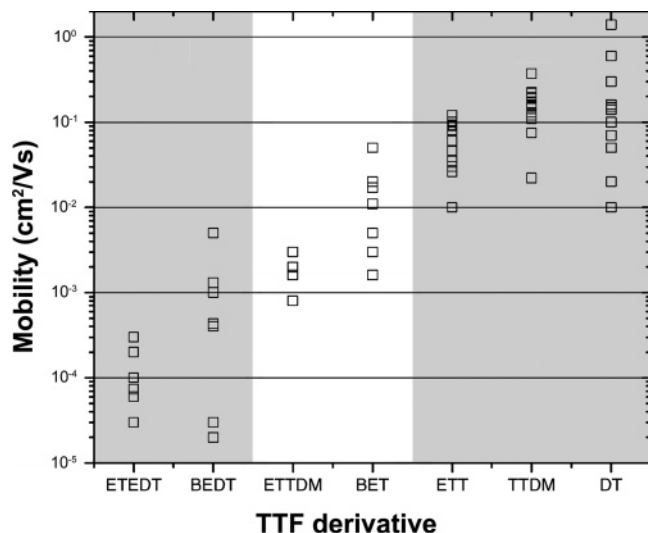
Figure 4. Illustration of the large variation in mobilities measured for various TTF derivatives. The results are plotted in three separate groups according to the crystal structure type (adapted from ref 83).

mobility data since intermolecular electronic couplings are very sensitive to the relative positions of the molecules.[74]

The herringbone structure is not a priori the most favorable packing for transport, in view of the large angle between the planes of adjacent molecules along the herringbone diagonal (which tends to reduce the strength of intermolecular interactions).[81] As a result, many efforts have been devoted to derivatizing the conjugated backbones in such a way as to generate crystal structures potentially more conducive to high carrier mobilities, in particular, structures where adjacent molecules are cofacial. This derivatization approach has been developed for instance by Anthony and co-workers for pentacene derivatives[82] and by Rovira and co-workers for tetrathiafulvalene (TTF) derivatives.[83] Unfortunately, such investigations cannot take much advantage of theoretical modeling, since quantum-chemistry and molecular-mechanics methods have not reached the stage yet where the crystal packing of even small organic molecules can be predicted reliably and accurately.[84,85]

Importantly, there is actually no clear demonstration that the types of cofacial packing that can be experimentally achieved lead to higher mobilities than an herringbone packing. The reason is that the molecules are never exactly superimposed on top of one another since a perfect cofacial situation is one in which electrostatic repulsion terms are largest. As a result, there usually occur displacements along the long and/or short molecular axes between adjacent molecules. Our theoretical investigations have shown that such displacements do strongly affect the intermolecular electronic couplings, in a way that intimately depends on the bonding-antibonding pattern of the frontier molecular orbitals (HOMO, highest occupied molecular orbital, or LUMO, lowest unoccupied molecular orbital).[74] Experimental data on single crystals of TTF derivatives show a large variation in mobility values as a function of packing, from 10^{-5} to 1 cm²/V·s, see Figure 4.[83] Changes in crystal packing are also responsible for crystallochromy, i.e., changes in the color of the crystal, which has been extensively studied for perylene derivatives.[86,87]

2.3.2. Disorder

Two kinds of disorder are usually distinguished:

Diagonal Disorder, which reflects the fluctuations in site energies (i.e., the energies of the HOMO or LUMO levels of individual molecules or chain segments) within the material; and

Off-Diagonal Disorder, which is related to fluctuations in the strength of interactions between adjacent molecules or chain segments, i.e., to modifications of their relative positions and orientations; off-diagonal disorder results in a distribution of electronic couplings within the material that can generate as well conducting pathways through the material as dead-ends for the charges.

In the case of flexible molecules/chains, a major contributor to diagonal disorder is conformational freedom, as it leads to a distribution of torsion angles between adjacent moieties. In polymer chains, such a distribution of torsion angles and/or the presence of chemical impurities result in diagonal disorder via the formation of finite-size conjugated segments with different lengths and therefore different HOMO and LUMO energies (we recall that the energy of the HOMO level destabilizes and that of the LUMO level stabilizes with conjugation length). In addition, diagonal disorder is induced by electrostatic/polarization effects from surrounding molecules, which vary with fluctuations in local packing; this effect is amplified when the molecules/chain repeat units contain local dipole moments;[88−91] this also holds true when the molecule or repeat unit as a whole carries no permanent dipole.[81] In theoretical simulations, energetic disorder is generally described via a Gaussian distribution of HOMO/LUMO level energies (see section 4.2); in conjugated polymers, the corresponding standard deviations are generally found to be on the order of 50−100 meV.[92,93]

That the degree of order intimately controls transport has been demonstrated for small molecules by tuning the amount of disorder via modifications of the deposition conditions (for instance, by changing the temperature or nature of the substrate, or the film thickness).[15,94] In the case of pentacene, varying the deposition conditions has been reported to lead to variations in charge mobility by up to 6 orders of magnitude.[95] Such a high sensitivity to experimental deposition conditions is a severe drawback in the study of charge transport since it often hampers a direct comparison between data collected by different groups.[9]

A qualitative illustration of the role of order is given by the evolution of charge carrier mobility in discotic or calamitic liquid crystalline materials. The example of hexathiohexyl triphenylene is illustrated in Figure 5.[28] The carrier mobility is observed to drop significantly in going from the crystalline phase to the mesophase and eventually to the isotropic phase.

The multiple trapping and release (MTR) model[9,96] has been introduced to describe situations where highly conducting regions coexist with traps linked to local structural disorder. In such instances, there appear localized states associated to the traps, located in energy below [above] the delocalized levels involved in bandlike transport for the electrons [holes]. Transport then operates via a succession of trapping events (with a probability assumed to be equal to 1) and thermal releases. It was demonstrated by Schmidlin[97] and Noolandi[98] that the MTR is a particular case of the general continuous time random walk (CTRW) model of Scher and Lax.[99] When the traps are homogeneously dispersed, the mobility is expressed as

$$\mu = \mu_0 \alpha \exp(-E_t/kT) \qquad (9)$$

where E_t is the trapping energy and α represents the ratio between the density of delocalized levels available for
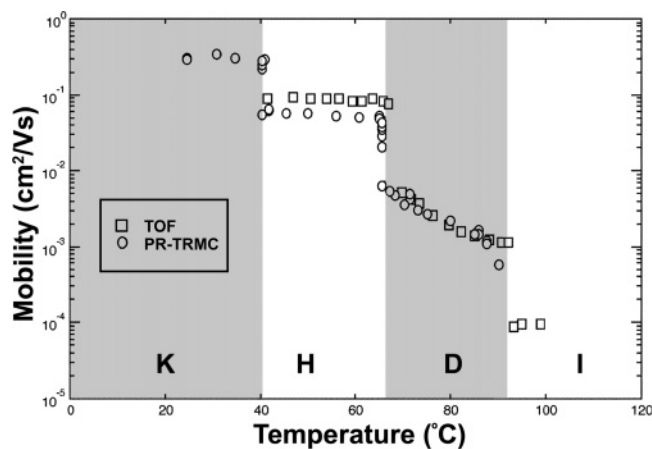
Figure 5. TOF Temperature dependence on heating of the 1D charge mobility in the hexakis(hexylthio) derivative of triphenylene determined by the PR−TRMC technique (circles) and the time-of-flight method (squares), as a function of the phase: crystalline solid (K), helical plastic phase (H), columnar mesophase (D), and isotropic liquid phase (I) (adapted from ref 28).

transport and the density of traps. In OFETs, applicability of the MTR model implies that the mobility is gate-voltage dependent and thermally activated.[100,101] When the traps are not homogeneously distributed but, for instance, are localized around grain boundaries in polycrystalline materials, the mobility can become temperature-independent; in that case, it is considered that the charges are actually able to tunnel across the structural defects.

The impact of grain boundaries on transport has been carefully examined for oligothiophenes in transistor configuration.[100] It was shown that mobility increases with grain size (the grain size can be altered by changing the substrate temperature during deposition). When transport takes place in both poorly and highly conducting regions and these regions can be modeled as being connected in series, the mobility is expressed as[100]

$$\frac{1}{\mu} = \frac{1}{\mu_{\text{low}}} + \frac{1}{\mu_{\text{high}}} \qquad (10)$$

Obviously, since $\mu_{\text{low}} \ll \mu_{\text{high}}$, this expression translates the fact that the mobility is limited by the poorly conducting regions.

The distribution of trap states can be accessed via thermally stimulated current (TSC) experiments. The sample is initially cooled to low temperature and the traps filled via carrier generation upon exposure to light; the sample is then progressively heated, which leads to the appearance of a current when the trapped charges are released.[102]

2.3.3. Temperature

The temperature dependence is markedly different in single crystals and in disordered materials. In single crystals, the hole and electron mobilities generally decrease with temperature according to a power law evolution: $\mu \div T^{-n}$. This is illustrated in Figure 6 for the case of electron and hole transport along a crystal axis direction of naphthalene. Similar evolution is observed along specific directions for a large number of single crystals; the main difference lies in the value of n, which typically varies between 0.5 and 3. This decrease in mobility with temperature is typical of band transport and originates from enhanced scattering processes by lattice phonons, as is the case for metals. The coupling
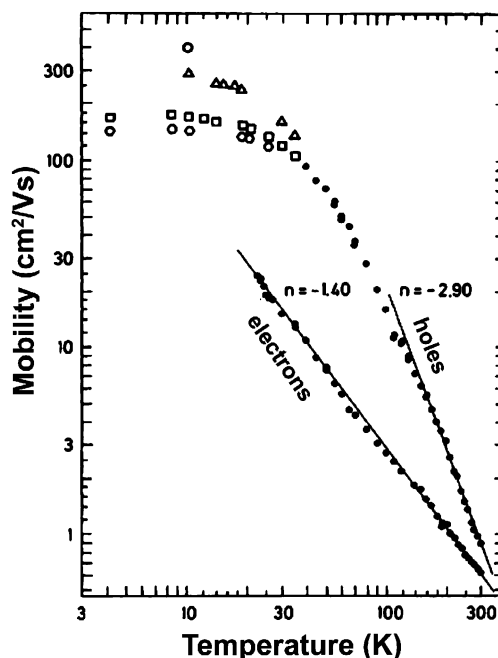
Figure 6. Log−log plot of the electron and hole mobilities in ultrapure naphthalene as a function of temperature. The applied electric field is approximately parallel to the crystallographic a direction (adapted from ref 33).

between the phonon modes and the carriers depends on the crystal packing; for instance, in the biphenyl crystal, electron transport below and above a structural phase transition is characterized by different n values.[94] Transport measurements on molecular single crystals indicate that charge mobilities as high as a few hundreds cm2/V·s can be attained at low temperature (up to 300 cm2/V·s for holes in naphthalene at 10 K)[33] and that electron and hole mobilities can be equally large. The latter point again confirms that the long-held belief in the field of organic electronics that electron transport is inefficient is a misconception (as discussed earlier, poor electron mobilities are most often due to extrinsic effects).

Mobilities in single crystals can sometimes significantly drop when the material is cooled below a critical temperature (for instance, around 30 K in perylene[94] and, depending on experimental conditions, around 160−180 K[42] or 250 K[40] in rubrene). Such a drop usually reflects the presence of traps with a depth (trapping energy) larger than $k_B T$ at the critical temperature. The presence of traps also reduces the mobility anisotropy.[42]

Interestingly, the temperature evolution of the mobility along directions where mobility is limited (for instance, between the herringbone layers) can display a power-law evolution at very low temperatures followed by a transition to a regime where mobility is nearly temperature independent. Such an evolution has been observed along the c-axis of ultrapure naphthalene single crystals around 100 K. A similar evolution is sometimes observed in crystals of lower purity.[103]

In highly disordered systems, transport generally proceeds via hopping and is thermally activated. Higher temperatures improve transport by providing the energy required to overcome the barriers created by energetic disorder. The temperature dependence has been often fitted to an Arrhenius-like law:

$$\mu_0 = \mu_\infty \exp(-\Delta/k_B T) \qquad (11)$$

where Δ is the activation energy and increases with the amount of disorder. In polyparaphenylenevinylene derivatives with very low mobilities ($<10^{-6}$ cm^2/V·s), Δ is estimated to be ca. 0.3−0.5 eV;[23] it is on the order of 0.13 eV for poly-3-hexylthiophene (P3HT) samples with mobilities in the range $10^{-4}/10^{-5}$ cm^2/V·s[104] and 0.02−0.04 eV for high-mobility P3HT samples with μ around 0.1 cm^2/V·s.[93] Δ values on the order of 0.1−0.2 eV have been reported from TOF measurements on calamitic liquid crystals.[105]

Note that that there is no full theoretical justification for such an Arrhenius-like expression. The theoretical simulations pioneered by Bässler and co-workers lead, in the presence of a Gaussian-type disorder, to a different expression:

$$\mu_0 = \mu_\infty \exp(-T_0/T)^2 \tag{12}$$

where T_0 describes the extent of energetic disorder. However, it turns out that both expressions generally fit the experimental data reasonably well within the limited temperature windows that are experimentally accessible.[18,23,105]

2.3.4. Electric Field

The electric-field dependence of mobility is also different in the case of single crystals and disordered materials. In single crystals, a field dependence is observed only in ultrapure crystals along the directions giving rise to the highest charge mobilities. In such instances, an increase in electric field is seen to reduce mobility.[33]

In disordered materials, an increase in mobility is observed at high fields. The field dependence in the range 10^4−10^6 V/cm generally obeys a Poole-Frenkel behavior:[106−108]

$$\mu(F) = \mu_0 \exp(\gamma \sqrt{F}) \tag{13}$$

where γ is temperature dependent and F denotes the electric field. The following expression for γ usually allows a good fit to the experimental data:[92,107]

$$\gamma = B\left[\frac{1}{k_B T} - \frac{1}{k_B T_0}\right] \tag{14}$$

where B is a constant characteristic of the system and T_0 is generally much larger than room temperature. However, a TOF study on P3HT chains has led to $T_0 = 250$ K;[106,109] this implies that γ becomes negative above T_0 and the mobility decreases with increasing electric field.[110] An understanding of this evolution can be found in the Bässler model[25] when off-diagonal disorder dominates diagonal disorder. Conceptually, this reflects the fact that, at low fields, the charges manage to follow the best percolation pathways and to avoid structural defects; higher electric fields impose a stronger directionality and prevent the charges from moving around the defects, thereby reducing mobility.

2.3.5. Impurities

Impurities in the present context refer to compounds that have a (slightly) different chemical structure than the compound nominally under investigation and that appear in small concentrations mainly as side products of the chemical synthesis. A major impact on the transport properties can be expected in particular when the frontier (HOMO/LUMO) molecular orbitals of the impurities have energies that fall within the HOMO−LUMO gaps of the pure molecules. One
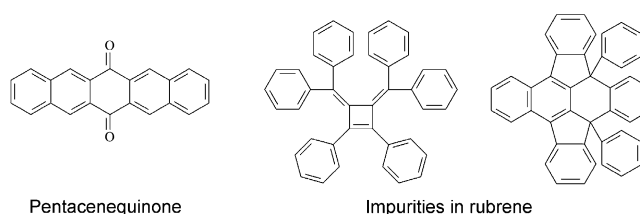
Figure 7. Chemical structures of impurities found in pentacene and rubrene.[32,42]

distinguishes between deep traps (when the trapping energy is much larger than $k_B T$) and shallow traps (when the trapping energy is on the order of $k_B T$, which allows for thermal detrapping).

In many instances, the exact nature of the impurities is difficult to determine. A recent work by Palstra and co-workers[32] has shown that the main impurities in pentacene single crystals are pentacene-quinone molecules (Figure 7); they are present in concentration around 0.7%. Purification steps allow to drop their concentration to about 0.07%, which significantly improves the hole mobility of pentacene single crystals (mobility values as high as 35 cm^2/V·s at room temperature and 58 cm^2/V·s at 225 K are obtained from SCLC measurements).[32] The nature of the impurities detected in tetracene single crystals has also been reported recently to correspond to quinone derivatives.[111] A recent investigation by Kloc and co-workers has also identified the nature of the two main impurities in the rubrene single crystal, see Figure 7.

2.3.6. Pressure

Application of an external pressure on a material is of fundamental interest as it can shed light into the structure-transport relationships. The application of hydrostatic pressure up to 0.3 GPa has been shown to increase the photocurrent linearly in tetracene and pentacene single crystals.[112] This evolution has been attributed to a reduction in intermolecular distances between adjacent molecules, as shown by the results of other pressure studies on organic conjugated molecules;[113] a sudden change in the evolution can be observed when a phase transition occurs.[112] Similarly, Bard and co-workers have reported a sharp increase in photocurrent in a stack of porphyrin derivatives when applying a pressure of 0.2 GPa by means of a cylindrical tip; this increase was assigned to a transition from a hopping regime to a band regime due to the increased intermolecular electronic coupling.[114]

2.3.7. Charge-Carrier Density

It is only recently that the influence of charge carrier density on mobility has been carefully examined. Blom and co-workers have shown experimentally that the hole carrier mobility in polyparaphenylenevinylene is markedly different when measured in transistor vs diode configuration (10^{-4} vs 10^{-7} cm^2/V·s, respectively).[115] The explanation lies in the fact that the density of injected charges is much larger in transistors than in diodes, see Figure 8; at lower densities, all the carriers can be affected by trapping due to energetic disorder and/or impurities; at higher carrier densities, only a portion of the carriers are necessary to fill all the traps and the remaining carriers can experience trap-free transport (however, it must be borne in mind that, when the filled traps are charged, they are expected to increase scattering, leading to observed mobility values lower than the intrinsic values).
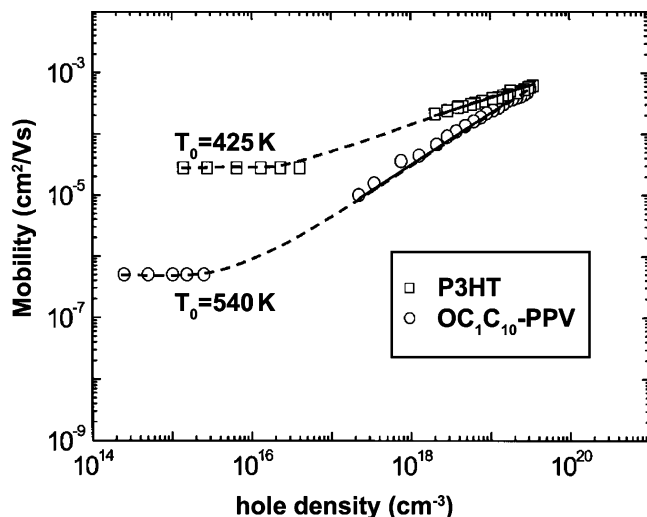
Figure 8. Mobility as a function of hole density in a diode and field-effect transistor for poly(3-hexyl thiophene) and poly(2-methoxy-5-(3′;7′-dimethyloctyloxy)-*p*-phenylene-vinylene) (adapted from ref 16).

The mobility was measured to be almost constant at low carrier density and to increase with a power-law dependence beyond 10^{16} cm^{-3}.[115]

2.3.8. Size/molecular Weight

Since the electronic coupling between adjacent molecules primarily depends on their packing, there exists no obvious relationship between molecular size and charge mobility. For instance, various TTF derivatives of similar molecular weight present a large dispersion in mobility values because of their different crystalline structures. Analysis of the size dependence would be much more meaningful for a series of analogous compounds with similar packings. Warman and co-workers have measured PR-TRMC charge mobilities for a series of discotic molecules that form quasi-1D stacks; they observed a negative linear semilogarithmic relationship between the maximum mobility obtained with a given conjugated core and the inverse number of carbon atoms in the core, which indicates in that instance that the larger the core, the larger the mobility.[27] However, such trends have to be taken with much caution since transport in discotic materials is found to be strongly influenced by the amplitude of the rotational angle between adjacent discs and the nature of the electroactive substituents attached to the core;[116] as a result, smaller conjugated cores can actually yield higher mobilities than larger ones. As will be emphasized again later, it is critical to bear in mind that the electronic coupling between adjacent molecules *is not* related to the degree of *spatial overlap* between adjacent molecules but rather to the degree of *wavefunction overlap* (which depends on the wavefunction bonding-antibonding pattern).[74]

The molecular weight of polymer chains can impact their transport properties. The hole mobility in regioregular P3HT chains is reported to increase by almost 4 orders of magnitude when the degree of polymerization goes from ∼20 to 220. This marked evolution was attributed to modifications in chain conformation and/or packing.[104,111] In particular, it was suggested that segments of long polymer chains can act as connectors between organized domains, which could rationalize the experimental increase in mobility with chain length; for smaller chains, the lower connectivity between crystalline domains translates into lower mobilities.

3. The Charge-Transport Parameters

In the absence of chemical and physical defects, the nature of charge transport depends on a subtle interplay between electronic and electron-vibration (phonon) interactions. In the case of the traditional, covalently bound inorganic semiconductors, the electron−phonon interactions are usually much smaller than the electronic interactions and simply account for the scattering of highly delocalized carriers. In contrast, in organic (macro)molecular semiconductors, the extensive experimental and theoretical investigations of the last decades have shown that the electron−phonon interactions are comparable to, or even larger than the electronic interactions (we recall that a phonon is a particle-like quantized mode of vibrational energy arising from the collective oscillations of atoms within a crystal). In such a case, electron−phonon coupling no longer plays the role of a perturbation but rather leads to the formation of quasi-particles, polarons, in which the electronic charge is dressed by phonon clouds.[38,117]

The origin and physical consequences of electronic and electron−phonon interactions can be understood by simply considering the tight-binding approximation. The corresponding electronic Hamiltonian is given by[38,117]

$$H_e = \sum_m \epsilon_m a_m^+ a_m + \sum_{mn} t_{mn} a_m^+ a_n \qquad (15)$$

Here, a_m^+ and a_m are the creation and annihilation operators, respectively, for an electron on lattice site m; ϵ_m is the electron site energy, and t_{mn} the transfer integral (electronic coupling). The site energy and the transfer integral are defined by the following equations:

$$\epsilon_m = \langle \varphi_m(\mathbf{r} - \mathbf{R}_m) | H_e | \varphi_m(\mathbf{r} - \mathbf{R}_m) \rangle \qquad (16)$$

$$t_{mn} = \langle \phi_m(\mathbf{r} - \mathbf{R}_m) | H_e | \phi_n(\mathbf{r} - \mathbf{R}_n) \rangle \qquad (17)$$

where vector $\mathbf{R}_m$ indicates the position of site m. For the sake of simplicity, in eqs 15−17, we have considered a single localized molecular orbital on each site, corresponding to the HOMO or LUMO for hole and electron transport, respectively. We note that orbitals φ_m in eqs 16 and 17 are assumed to be orthogonal; however, this is usually not the case for the HOMOs or LUMOs placed on different sites/molecules. We will come back to the nonorthogonality issue in section 3.1.2 and discuss how ϵ_m and t_{mn} transform when going from nonorthogonal to orthogonal representation.

It is well-established that the electronic, optical, and transport properties[4,50,118−124] are very sensitive to the details of the system environment, molecular geometry, intermolecular distance, and molecular packing. As a result, any small displacement of atoms from their equilibrium positions affects the microscopic parameters; it is precisely this dependence of the system parameters on vibration (phonon) coordinates that is referred to as electron−phonon coupling.

In organic molecular crystals, the weak van der Waals interactions between molecules generally have only a small effect on the *intra*-molecular properties. Thus, it is convenient to start by distinguishing between *intra*-molecular (internal) and *inter*-molecular (external) vibrational degrees of freedom and to consider the effects arising from their hybridization in a later step. From eq 15, two distinct sources of electron−phonon interactions can be found. First, the site energy ϵ_m is modulated by *intra*-molecular vibrations, which leads to

electron−vibration interactions with such modes. In addition, ϵ_m is affected by the surrounding (crystal) potential and is thus modulated as well by *inter*-molecular vibrations. The electron−vibration coupling arising from the overall modulations of the site energy is termed *local* coupling; it is the key interaction present in Holstein's molecular crystal model.[125,126] The second source of electron−phonon interaction is related to the dependence of the transfer integral, t_{mn}, on the spacing and relative orientations of adjacent molecules. The modulation of the transfer integrals by lattice phonons is referred to as *nonlocal* coupling;[127−132] this coupling constitutes the major interaction in Peierls-type models,[133] such as the Su−Schrieffer−Heeger Hamiltonian that has been largely applied to conducting polymers.[1] In organic molecular systems, both local and nonlocal electron−phonon interactions are generally important.

The Hamiltonian including the electron−phonon interaction is obtained by expanding ϵ_m and t_{mn} in a power (or Taylor) series of the phonon coordinates (see section 3.2).[134] In the linear electron−phonon coupling approximation, the system Hamiltonian is given by[38,117]

$$H = H_e + H_{ph} + H_{e-ph}^l + H_{e-ph}^{nl} \tag{18}$$

$$H_e = \sum_m \epsilon_m^{(0)} a_m^+ a_m + \sum_{mn} t_{mn}^{(0)} a_m^+ a_n \tag{19}$$

$$H_{ph} = \sum_{\mathbf{q}j} \hbar\omega_{\mathbf{q}j}\left(b_{\mathbf{q}j}^+ b_{\mathbf{q}j} + \frac{1}{2}\right) \tag{20}$$

$$H_{e-ph}^l = N^{-1/2}\sum_{\mathbf{q}j}\sum_m \hbar\omega_{\mathbf{q}j}[g_m(\mathbf{q},j)b_{\mathbf{q}j} + g_m^*(\mathbf{q},j)b_{\mathbf{q}j}^+]a_m^+ a_m \tag{21}$$

$$H_{e-ph}^{nl} = N^{-1/2}\sum_{\mathbf{q}j}\sum_m\sum_{n\neq m} \hbar\omega_{\mathbf{q}j}[g_{mn}(\mathbf{q},j)b_{\mathbf{q}j} + g_{mn}^*(\mathbf{q},j)b_{\mathbf{q}j}^+]a_n^+ a_m \tag{22}$$

Here, $\epsilon_m^{(0)}$ and $t_{mn}^{(0)}$ are the parameters obtained at a reference (usually equilibrium) configuration. N denotes the total number of unit cells. H_{ph} is the Hamiltonian of the phonon subsystem with $b_{\mathbf{q}j}^+$ and $b_{\mathbf{q}j}$ denoting the creation and annihilation operators for a phonon of branch j with energy $\hbar\omega_{\mathbf{q}j}$ and wavevector $\mathbf{q}$. We recall that, in crystals with s atoms present in the unit cell, the phonon excitation spectrum contains 3s branches (dispersion curves). Among these, there occur three branches for which $\hbar\omega_{\mathbf{q}j} \rightarrow 0$ as $\mathbf{q} \rightarrow 0$; these are referred to as acoustical. The other branches have finite frequencies at $\mathbf{q} = 0$, are classified as optical phonon branches, and include the *intra*-molecular vibrations.[135,136] For the sake of better understanding, the electron−phonon interaction (H_{e-ph}) has been split into local and nonlocal contributions in eqs 21 and 22, respectively. The $g_m(\mathbf{q}, j)$ and $g_{mn}(\mathbf{q}, j)$ terms denote the corresponding local and nonlocal electron−phonon coupling constants. Below, we outline the present state-of-the-art in the derivation of electronic and electron−phonon coupling constants from quantum-chemical calculations.

We note that the electron−phonon interactions produce a time-dependent variation of the transport parameters and thus introduce a dynamic disorder. The impact of static disorder can be easily incorporated in the model by considering a time-independent distribution (usually taken as Gaussian) for

parameters $\epsilon_n^{(0)}$ and $t_{mn}^{(0)}$; as briefly discussed in section 2.3, these sources of static disorder are referred to as diagonal disorder (involving only terms where $n = m$) and off-diagonal disorder ($n \neq m$).[38] The same classification can be applied to the dynamic contributions; local and nonlocal electron−phonon couplings correspond to diagonal and off-diagonal dynamic disorder mechanisms, respectively. The role of both static and dynamic disorder effects on charge transport is discussed in section 4.

We now turn to a discussion of the terms present in the Hamiltonian of eq 18, starting with the electronic coupling matrix elements.

3.1. Electronic Coupling

The charge-transport properties strongly depend on the extent of electronic coupling. Most rigorously, the magnitude of this interaction is defined by the matrix element $t_{ab} = \langle\Psi_a|H|\Psi_b\rangle$, where H is the electronic Hamiltonian of the system and Ψ_a and Ψ_b are the wavefunctions of two charge-localized states (diabatic states), i.e., the states obtained in the hypothetical absence of any coupling between the molecular units.[137] For instance, in the case of two interacting oligomers (M_a and M_b) carrying an excess charge, the diabatic states correspond to the two localized valence structures $M_a^+-M_b$ and $M_a-M_b^+$ (or $M_a^--M_b$ and $M_a-M_b^-$). The determination of the diabatic states is in general a very challenging task; as a result, it is customary to rely on a transformation to an adiabatic basis, Ψ_1 and Ψ_2, that can be directly assessed by means of quantum-chemical calculations (in contrast to the diabatic representation, the adiabatic representation is diagonal with respect to the electronic Hamiltonian).

3.1.1. The Energy-Splitting-in-Dimer Method

The issue of determining accurate electronic coupling (tunneling matrix element) values has long received significant attention in many areas of biology, chemistry, and physics.[137−149] The most simple approach, which has been widely used to evaluate electronic couplings in organic semiconductors, is referred to as the "energy splitting in dimer" (ESD) method.[116,122,123,137,150−156] It is based on the realization that at the transition point, where the excess charge is equally delocalized over both sites (symmetric dimer), the energy difference $E_2 - E_1$ between the adiabatic states Ψ_1 and Ψ_2 corresponds to $2t_{ab}$; as a result, $t_{ab} = (E_2 - E_1)/2$. Rigorously, the method requires the use of the geometry at the transition state (i.e., at the avoided crossing point) of the charged dimer. In practice, the calculations are simplified by either considering the geometry of the neutral dimer or the geometry obtained as the average over the neutral and ionic nuclear coordinates of the monomers.[74,122,123,150,157−159]

Another major simplification is to apply Koopmans' theorem (KT),[160] that is, to rely on the one-electron approximation. In this context, the absolute value of the transfer integral for electron [hole] transfer from M_a to M_b is approximated as

$$t = \frac{\epsilon_{L+1[H]} - \epsilon_{L[H-1]}}{2} \tag{23}$$

where $\epsilon_{L[H]}$ and $\epsilon_{L+1[H-1]}$ are the energies of the LUMO and LUMO+1 [HOMO and HOMO-1] levels taken from the closed-shell configuration of the neutral state of a dimer (M_a-M_b). Because of its simplicity, the KT-ESD approach

is currently the most frequently used method for the estimation of transfer integrals in organic semiconductors. Recent studies have shown that the KT estimates are in good agreement with the results derived from electron-correlated CAS-PT2 (second-order perturbation theory based on CASS-CF) and CAS-SI (CASSCF-State Interaction) calculations.[161,162]

3.1.2. The Orthogonality Issue

In the one-electron approximation, the diabatic states are associated with localized monomer orbitals, $\tilde{\varphi}_i$. The transfer integrals and site energies can then be computed directly as[81,163]

$$\tilde{\epsilon}_i = \langle \tilde{\varphi}_i | \hat{\mathbf{H}} | \tilde{\varphi}_i \rangle \tag{24}$$

$$\tilde{t}_{ij} = \langle \tilde{\varphi}_i | \hat{\mathbf{H}} | \tilde{\varphi}_j \rangle \tag{25}$$

The matrix elements $\tilde{\epsilon}_i$ and $\tilde{t}_{ij}$ have the same physical meaning as the parameters ϵ_i and t_{ij} in eq 15; however, these two sets of parameters are not identical. Indeed, while the monomer orbitals $\tilde{\varphi}_i$ used to derive $\tilde{\epsilon}_i$ and $\tilde{t}_{ij}$ are nonorthogonal, eq 15 assumes an orthogonal basis, φ_i. To illustrate the orthogonality issue, we compare below the dimer energy splittings $\Delta E_{12} = \epsilon_H - \epsilon_{H-1}$ obtained using both nonorthogonal and orthogonal basis sets. Assuming that the dimer HOMO and HOMO-1 result from the interaction of only monomer HOMOs, ΔE_{12} in the nonorthogonal basis is given by

$$\Delta E_{12} = \frac{\sqrt{(\tilde{\epsilon}_2 - \tilde{\epsilon}_1)^2 + 4(\tilde{t}_{12}^2 - \tilde{t}_{12}S_{12}(\tilde{\epsilon}_2 + \tilde{\epsilon}_1) + \tilde{\epsilon}_2\tilde{\epsilon}_1S_{12}^2)}}{1 - S_{12}^2} \tag{26}$$

where S_{12} is the spatial overlap integral between the HOMOs of the two monomers. To generate an orthonormal basis set (φ_i) that maintains as much as possible the initial local character of the monomer orbitals, Löwdin's symmetric transformation can be applied to the $\tilde{\varphi}_i$ levels.[164] In a symmetrically orthonormalized basis, eq 26 takes the form[81]

$$\Delta E_{12} = \sqrt{(\epsilon_1 - \epsilon_2)^2 + 4t_{12}^2} \tag{27}$$

where

$$\epsilon_{1(2)} = \frac{1}{2} \frac{(\tilde{\epsilon}_1 + \tilde{\epsilon}_2) - 2\tilde{t}_{12}S_{12} \pm (\tilde{\epsilon}_1 - \tilde{\epsilon}_2)\sqrt{1 - S_{12}^2}}{1 - S_{12}^2} \tag{28}$$

$$t_{12} = \frac{\tilde{t}_{12} - \frac{1}{2}(\tilde{\epsilon}_1 + \tilde{\epsilon}_2)S_{12}}{1 - S_{12}^2} \tag{29}$$

The fact that eq 26 reduces to $\Delta E_{12} = 2\tilde{t}_{12}$ only when $S_{12} = 0$ and $\tilde{\epsilon}_2 = \tilde{\epsilon}_1$ might at first sight suggest that the ESD approach does not account for spatial overlap and therefore the transfer integrals estimated in this way could substantially deviate from the actual values. However, eqs 16−17 and 26−29 show that the ESD method can be interpreted as if an orthogonal diabatic basis set were explicitly employed, so that the transfer integral t_{ij} has the meaning of an effective quantity that accounts for both $\tilde{t}_{ij}$ and S_{ij}.

The calculations performed with either an orthogonal or nonorthogonal basis set yield the same physical observables. However, the use of an orthogonal representation is more suitable to build and handle model Hamiltonians such as the tight-binding model. In addition, the transfer integrals defined in a nonorthogonal basis set depend on the choice of energy origin.[165] Indeed, an electronic Hamiltonian that differs from the initial Hamiltonian by a constant ($H \rightarrow H + C$) yields transfer integrals that are shifted from their initial values as $\tilde{t}_{ij} \rightarrow \tilde{t}_{ij} + CS_{ij}$.[165] Since the site energies also experience an energy shift $\tilde{\epsilon}_i \rightarrow \tilde{\epsilon}_i + C$, it is seen from eq 29 that the parameters t_{ij} defined in an orthogonal basis set are invariant under such an Hamiltonian transformation. Therefore, when quantitative comparisons of electronic interactions are made only in terms of transfer integrals, the use of an orthogonal basis is more appropriate.

3.1.3. Impact of the Site Energy

Equation 27 shows that the transfer integral t_{12} can be estimated as half of ΔE_{12} only when the site energies ϵ_i are equal. Although the fact that ΔE_{12} can be affected by site energies has been previously discussed in the literature, this dependence was solely attributed to chemical or geometric differences between the two molecules. We have shown recently[81] that there is another contribution to the site energy difference $\Delta\epsilon_{12} (= \epsilon_2 - \epsilon_1)$ that results from the polarization of the localized electronic states by intermolecular interactions. This contribution has often been overlooked, especially when dealing with systems formed from identical monomers. The usual assumption is that the site energies of identical monomers are the same; however, this assumption can turn out to be wrong when intermolecular interactions are taken into account, which can be easily understood from symmetry considerations. The energy difference $\Delta\epsilon_{12}$ vanishes only when the two localized valence structures $M_a^+-M_b$ and $M_a-M_b^+$ can be obtained from one another by a symmetry transformation, that is, when the dimer is symmetric. Otherwise, when the two molecules are not equivalent by symmetry, the molecules affect each other differently and the site energy difference is nonzero. In this case, the ESD approach can drastically overestimate the transfer integral. It is also important to note that, even when two molecules are equivalent in the crystal environment, this is no longer necessarily the case when the corresponding dimer is taken out of the crystal.

Figure 9 illustrates the potential problem that can arise from the blind use of the ESD method to estimate transfer integrals. We consider the simple example of an ethylene dimer where one monomer is tilted around its longitudinal molecular axis. The calculation of $\Delta E_{12}/2$ at the density functional theory (DFT) level provides only a slight variation with tilt angle; ΔE_{12}, and thus the transfer integral when taken as $\Delta E_{12}/2$, is predicted to reach its maximal value at the face-to-edge configuration.[81] However, the direct calculations by means of eq 29 show that the transfer integral gradually decreases with the tilt angle, from its maximum value at the cofacial orientation to exactly zero when the system reaches the face-to-edge configuration. In contrast, the site energy difference $\Delta\epsilon_{12}$ follows the opposite trend. As a consequence, in the face-to-edge configuration, $\Delta\epsilon_{12}$ is actually the sole contributor to the energy splitting ΔE_{12}. Note also that, for this situation, the transfer matrix element is a quadratic function of the torsional coordinates; this underlines that taking account of the quadratic electron−phonon coupling
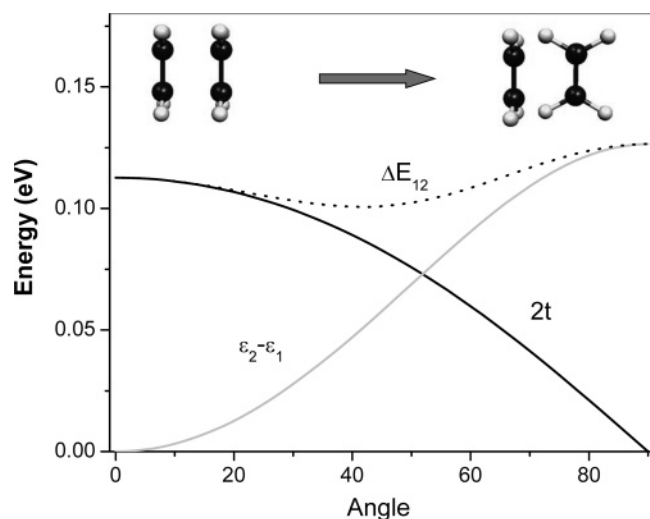
Figure 9. Evolution of the energy splitting (dotted line), transfer integral (black line), and site energy difference (gray line) as a function of the rotation of one ethylene molecule with respect to the other around its long molecular axis (adapted from ref 81).

could prove to be important in certain situations, such as torsional motions.[134,166,167]

This significant polarization-induced effect in the face-to-edge dimers should not be surprising. A simple rationalization is that the slightly positively charged hydrogens of the "edge" molecule lower the energy of the π-type HOMO of the "face" molecule. We have tested this hypothesis by computing the orbital energies of each ethylene in the dimer with the other molecule represented by point charges derived from the monomer calculation. The site energies estimated in this way are found to be in good agreement with the quantum-mechanical calculations using eq 28.[81] This result underscores the classical electrostatic origin of the site energy difference $\Delta\epsilon_{12}$.

We note that, in the present neutral dimer approach, these electrostatic contributions arise from the interactions between the orbitals of one molecule and the permanent multipole moments of the other molecule. Therefore, when such quantities are of interest, the values for the site energies ϵ_i should be obtained on the basis of calculations that explicitly include the charged site into the model to account for the contributions due to the *induced* dipole and higher multipole moments.

3.1.4. Electronic Coupling in Oligoacene Derivatives

We now turn to a description of electronic couplings calculated in the framework of the approach discussed above. We focus on hole transport in a few systems of interest: naphthalene, anthracene, tetracene, rubrene, and pentacene. Here, the calculations are based on DFT with the PW91 functional and the triple-ζ plus polarization (TZP) basis set. As was shown previously for pentacene[81] and ethylene[150] dimers, the TZP basis set yields reliable results vs larger basis sets.

We first consider several dimers along various crystal directions using the crystallographic parameters presented in Table 1. The results are summarized in Table 2 (we note that the DFT results are generally similar to the previously reported INDO/S values).[74,152] As seen from Table 2, the transfer integrals are larger in the crystals of the more extended oligomers, which points to wider bands in the latter.[152] The largest transfer integrals, 0.083 and 0.084 eV,

Table 1. Crystallographic Parameters for the Unit Cells of Oligoacenes[71,174,175] and Rubrene[176]

|	a^a	b	c	α^b	β	γ
naphthalene	8.098	5.953	8.652	90.00	124.40	90.00
anthracene	8.414	5.990	11.095	90.00	125.29	90.00
tetracene	6.057	7.838	13.010	77.13	72.12	85.79
pentacene	6.275	7.714	14.442	76.75	88.01	84.52
rubrene	7.184	14.433	26.897	90.00	90.00	90.00

^{a} Units in Å. ^{b} Units in deg.

Table 2. DFT-Calculated Transfer Integrals in Oligoacenes (in meV)

a	b	c	naphthalene	anthra-cene	tetra-cene	penta-cene	rubrene
1	0	0	0	0	−4/16	37/34	83
0	1	0	−35	−44	0	0	0
0	0	1	0	0	0	0	0
1/2	1/2	0	−8	−23	−23	85	15
−1/2	1/2	0	−8	−23	70	−51	15

are derived for the (1, 0, 0) and (1/2, 1/2, 0) directions in rubrene and pentacene, respectively. We note that these estimates are of the same order of magnitude as the experimental data recently reported for pentacene thin films[168] and fluorene dimers.[169]

It is useful to stress that a blind application of the ESD approach for dimers along the diagonal directions within the *ab*-plane (herringbone layer) would lead to a significant overestimation of the electronic couplings. For instance, in the case of pentacene, the ESD $\Delta E_{12}/2$ calculations would result in estimates of 0.214 and 0.189 eV for the electronic couplings along the (1/2, 1/2, 0) and (−1/2, 1/2, 0) directions; these values are about three times as large as the t_{12} values of 0.084 and 0.050 eV. The electronic coupling in oligoacene and other organic crystals have been recently probed by means of DFT band-structure calculations.[170−173] The fit of the band-structure results to a tight-binding model yields transfer integrals for pentacene[171] that are comparable to the ESD estimates. In contrast, in oligothiophene systems,[172] the couplings derived from DFT band-structure calculations were found to be somewhat smaller than the ESD values obtained at the INDO/S level of calculations. We note, however, that a thorough comparison between these two approaches has not been reported yet.

The transfer integrals strongly depend on the mode of packing. We have previously demonstrated that even small molecular displacements can lead to significant changes in transfer integrals.[4,74,116,123] This sensitivity of the transfer integrals to intermolecular separations and orientations is illustrated in the case of tetracene in Figures 10 and 11. Figure 10 shows the evolution of the electronic splittings for a perfectly cofacial tetracene dimer as a function of intermolecular distance. Although fully cofacial configurations are rarely encountered in actual crystal structures, it is of interest to study such geometries as they provide a high-symmetry reference point and an upper limit for the electronic couplings. The electronic couplings are observed to decay exponentially with intermolecular distance; this simply translates the exponential decay of intermolecular overlap between the π-atomic orbitals when the two oligomers are pulled apart. It is important to realize that the electronic couplings can vary by as much as a factor of 3−4 between 3.4 and 4.0 Å, that is, within the typical range of intermolecular distances found in organic conjugated crystals and thin films.
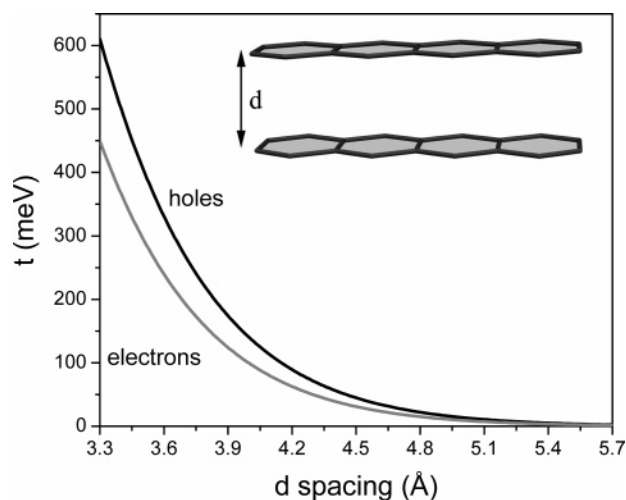
Figure 10. Evolution of the INDO-calculated transfer integrals for electron and hole transfer in a tetracene cofacial dimer, as a function of intermolecular distance.

Figure 11 describes the evolution of the hole and electron transfer integrals in cofacial dimers when one of the tetracene molecules is translated along its long or short axis. As expected, the overall effect of such displacements is to reduce the wavefunction overlap and thus the electronic coupling. However, the most interesting result is the appearance of oscillations in the values of the couplings for translations along the long molecular axis. As a consequence of the differences in oscillation periods for electron and hole transfer integrals, even small translations can lead to situations where the couplings for electrons are larger than for holes and hence where electrons can possibly be more mobile than holes. The calculated evolutions can be rationalized in terms of the phase and nodal properties of the HOMO and LUMO orbitals of a single tetracene molecule.[74] In the HOMO level, for instance, the distribution of the positive and negative linear combination of atomic orbitals (LCAO) coefficients shows a change in the sign of the wavefunction for every benzene ring. This pattern leads to extrema in the calculated electronic splittings for degrees of translation along the long molecular axis roughly corresponding to multiples of the ring size. Another interesting result is obtained in the case of translations along the short molecular axis. As seen from Figure 11, both hole and electron transfer integrals vanish only for translations over 6.0 Å, which actually corresponds to more than twice the lateral width of the carbon backbone of the tetracene molecule. These observations highlight that estimates of the electronic coupling purely based on the "spatial overlap" between the two molecules can be very misleading.

Two major conclusions can be drawn from these results: (i) The critical parameter in determining the electronic couplings is the wavefunction overlap. (ii) The marked dependence of the transfer integrals on small molecular displacements point to the significance of nonlocal electron−phonon couplings (vide infra).

3.2. Electron−Phonon Interactions

3.2.1. Internal and External Vibrations

The current level of quantum-chemical methods, in particular, those based on DFT, provides a reliable description of the *intra*-molecular (internal) vibrational spectra of organic molecules ranging from small to relatively large. However, calculating the vibrational modes in an organic molecular crystal is a much more complicated proposition. This is because conventional first-principles methods fail to describe weak intermolecular interactions adequately. For instance, DFT full geometry optimizations lead to unphysical expansions of the unit cell. This issue can be somewhat overcome by constraining the cell parameters to the experimental values;[177−183] the calculations performed for several systems[153,177−183] indicate that the differences between the experimental geometry and the optimized geometry obtained using constrained unit-cell parameters are insignificant. In addition, the phonon spectra in benzene[177] and thiophene-based crystals[178] obtained in this framework compare well with inelastic neutron scattering data. While we can expect that an increasing number of first-principles investigations on the lattice dynamics of organic molecular crystals will appear in the near future, current studies remain based on empirical potential energy models (force fields), in which intermolecular interactions are described by empirical atom−atom potentials;[118,184−191] such calculations in many cases make use as well of the rigid-body approximation, in which the intramolecular geometries are frozen.

The rigid-body approximation finds its justification in the fact that, as a result of weak *inter*-molecular interactions, the restoring forces for *intra*-molecular deformations are much larger than those related to changes in intermolecular arrangements. Therefore, to a first approximation, the separation between the internal and external degrees of freedom of the molecule is retained in the crystal. This model significantly simplifies the calculations and leads to a more intuitive physical picture, since external lattice modes make the molecules move as a whole around their equilibrium positions in the form of translational and rotational (libration) oscillations.[136] Applicability of the rigid-body approximation requires that the frequencies of the internal modes be very close to the frequencies of the molecules in the gas phase.

The normal coordinates $Q_j(n)$ of a molecule located at lattice site n and the internal phonon coordinates $Q(\mathbf{q}, j)$ are related through the expression[134]

$$Q_j(n) = N^{-1/2}\sum_{\mathbf{q}}e^{i(\mathbf{qR}_n)}Q(\mathbf{q}, j) \qquad (30)$$
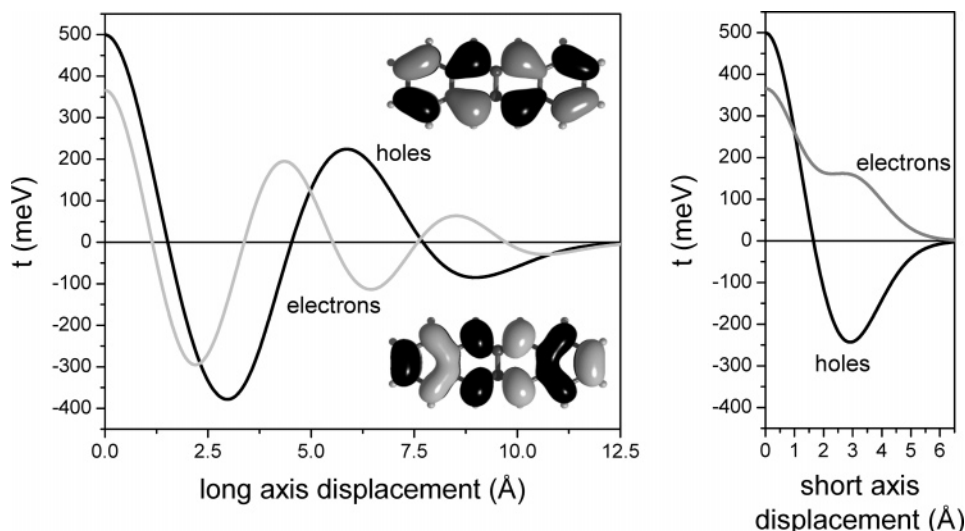
The transformation to second-quantization representation is obtained by making the following substitution:[136]

$$Q(\mathbf{q}, j) = \sqrt{\frac{\hbar}{2M_j\omega_{\mathbf{q}j}}}(b_{\mathbf{q}j} + b_{-\mathbf{q}j}^{+}) \qquad (31)$$

where M_j is the reduced mass of mode Q_j. As follows from our earlier discussion, the internal phonon modes are optical in character.

In addition to intramolecular vibrations, each molecule is characterized by six external coordinates comprising three translations and three rotations. Therefore, in the rigid-body approximation, for each value of vector $\mathbf{q}$, there exist 6s lattice modes, where s denotes the number of molecules per unit cell; among these modes, three are acoustic modes and the other 6s-3 modes are optical. The external coordinates can be written in terms of the creation and annihilation operators as[184]

$$u_{n,\alpha,\beta} = \sum_{\mathbf{q}j}\sqrt{\frac{\hbar}{2M_{\beta}N\omega_{\mathbf{q}j}}}\xi_{\alpha\beta}(\mathbf{q}, j)e^{i(\mathbf{qR}_n)}(b_{\mathbf{q}j} + b_{-\mathbf{q}j}^{+}) \quad (32)$$

Figure 11. Evolution of the INDO-calculated transfer integrals for electron and hole transfer in a tetracene cofacial dimer, as a function of the degree of translation of one molecule along its long axis (left) and short axis (right); the intermolecular distance is set at 3.74 Å (which is the intermolecular separation found in the rubrene crystal along the *a*-direction).[176] The HOMO (top) and LUMO (bottom) wavefunctions are presented as well in the figure on the left.

Here, the $\xi_{\alpha\beta}$ terms represent the vibrational amplitudes with $\alpha = 1$ to 3s and $\beta = 1$ to 6; β enumerates the generalized displacements (translational: $\beta = 1$ to 3; and rotational: $\beta = 4$ to 6); therefore, for $\beta = 1-3$, M_β represents the molecular mass and, for $\beta = 4$ to 6, M_β represents the molecular moment of inertia around the corresponding principal axis. The lattice phonon frequencies and vibrational amplitudes are obtained by standard diagonalization of the related dynamic matrix.[135,136]

3.2.2. Local Electron–Phonon Coupling

When just keeping the local electron−phonon coupling ($g_{nm} = 0$) in eq 18, the standard Holstein-type polaron model is obtained.[125−128] The physical meaning of the local coupling constants can be readily understood by considering the limiting case of weak electronic coupling ($t_{mn} = 0$). In this case, the Hamiltonian for a single charge carrier in the lattice can be diagonalized exactly with the resulting energy given by[117]

$$E_m = \epsilon_m^{(0)} - \frac{1}{N}\sum_{\mathbf{q}j}\hbar\omega_{\mathbf{q}j}|g_m(\mathbf{q}, j)|^2 + \sum_{\mathbf{q}j}\hbar\omega_{\mathbf{q}j}\left(n_{\mathbf{q}j} + \frac{1}{2}\right)$$

(33)

The electron (hole) is localized on a single lattice site with a stabilization energy referred to as the polaron binding energy, E_{pol}:

$$E_{pol} = \frac{1}{N}\sum_{\mathbf{q}j}\hbar\omega_{\mathbf{q}j}|g_m(\mathbf{q}, j)|^2$$

(34)

The polaron binding energy results from the deformations in molecular and lattice geometries that occur as the carrier localizes on a given site. This quantity is thus closely related to the reorganization energy in electron-transfer theories. The contribution to the polaron binding energy arising from the internal degrees of freedom can be obtained by expanding the site energy ϵ_m in powers of molecular normal-mode
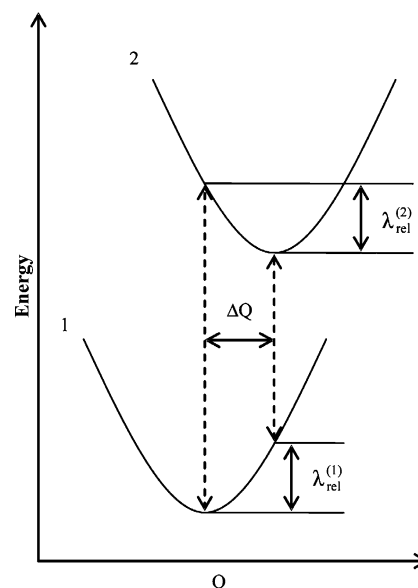
Figure 12. Sketch of the potential energy surfaces for neutral state 1 and charged molecule state 2, showing the vertical transitions (dashed lines), the normal mode displacement ΔQ, and the relaxation energies $\lambda_{rel}^{(1)}$ and $\lambda_{rel}^{(2)}$.

coordinates, $Q_m(j)$. In the harmonic approximation, we obtain

$$\epsilon_m(Q) = \epsilon_m^{(0)} + \sum_j V_m(j)Q_m(j) + \frac{1}{2}\sum_j M_j\omega_j^2\,Q_m^{\,2}(j) \quad (35)$$

where

$$V_m(j) = \left(\frac{\partial\epsilon_m}{\partial Q_m(j)}\right)_{Q=0}$$

(36)

Since ϵ_m is the energy of a frontier molecular orbital (HOMO and LUMO for hole and electron transport, respectively), eq 35 actually represents the adiabatic potential surface of the charged molecule obtained in the one-electron picture (Koopmans' theorem).[160] Figure 12 shows the potential energy surfaces for electronic states 1 and 2, which cor-

respond to the neutral state and the ground state of the charged molecule. Assuming that the normal vibrational modes of both states are the same, the geometry relaxation energies occurring upon vertical transition from the neutral state to a charged state and vice versa ($\lambda_{rel}^{(2)}$, $\lambda_{rel}^{(1)}$) are equal and given by

$$\lambda_{rel} = \sum_j \lambda_j = \sum_j \frac{V^2(j)}{2M_j\omega_j^2} \tag{37}$$

(note that, since all molecules have identical vibrational Hamiltonians, we have dropped the index (m) that labels the molecules). By making use of eqs 30, 34, 36, and 37, we obtain that $E_{pol} = \lambda_{rel}$, i.e., the *intra*-molecular contribution to the polaron binding energy is equal to the geometry relaxation energy upon charging the molecule. We note that translation symmetry requires that $g_m(\mathbf{q}, j) = e^{i\mathbf{q}\mathbf{R}_m}g(\mathbf{q}, j)$.[127,128,192] Furthermore, the internal optical phonon modes are assumed to be dispersionless; therefore, the coupling constant $g(\mathbf{q}, j)$ does not depend on the phonon wavevector $\mathbf{q}$, that is, $g(\mathbf{q}, j) = g(j)$. By comparing eq 37 with eq 34, we obtain

$$g^2(j) = \frac{V^2(j)}{2M_j\hbar\omega_j^3} = \frac{\lambda_j}{\hbar\omega_j} \tag{38}$$

It is useful to point out that $g(j)$ is directly related to the Huang–Rhys factor $S_j = g^2(j)$; this dimensionless factor is commonly used in molecular spectroscopy and electron-transfer theory.

As discussed in more detail elsewhere,[4,193,194] the intramolecular reorganization energy (λ_{reorg}) associated with an *inter*-molecular electron-transfer reaction of the type $M_a^- - M_b \rightarrow M_a - M_b^-$, is given by

$$\lambda_{reorg} = \lambda_{rel}^{(1)} + \lambda_{rel}^{(2)} \tag{39}$$

Thus, within the approximations described above, the polaron binding energy is equal to half the reorganization energy, i.e., $E_{pol} = \lambda_{reorg}/2$.

The electron-vibration coupling constants can be evaluated directly by using eq 36 and computing the respective derivatives numerically.[195–197] The advantage of this approach is that, by taking the geometry of the neutral molecule as a reference, only the normal modes of this state are required. An alternate approach, widely used in our group, is based on geometry optimizations and normal-mode calculations of both the neutral and charged molecular states.[116,123,153,193,194,198–201] The partition of the total relaxation (polaron) energy into the contributions from each vibrational mode is given by

$$E_{pol} = \lambda_{rel} = \sum_j \lambda_j = \sum_j \frac{M_j\omega_j^2\Delta Q_j^2}{2} \tag{40}$$

Here, ΔQ_i represents the displacement along normal mode Q_i between the equilibrium geometries of the neutral and charged molecules; as seen from eqs 37, 38, and 40, the vibronic coupling constant $g(j)$ and $V(j)$ can be easily obtained from the displacements ΔQ_i. Since this approach is based on total energy calculations for the neutral and charged states, it goes beyond the one-electron approxima-
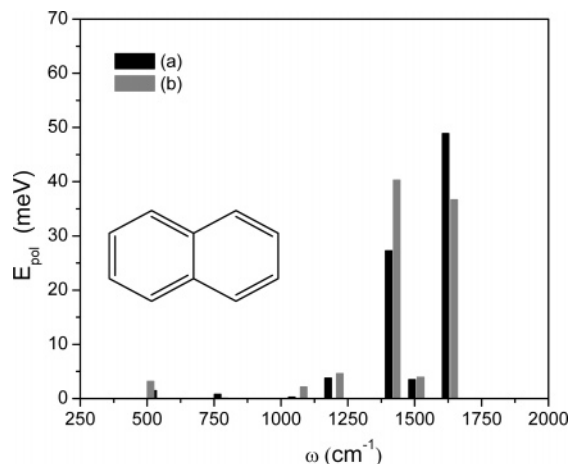
Figure 13. B3LYP/6-31G** estimates of the vibrational couplings in naphthalene derived by means of eq 36 (a) and eq 40 (b); see text for discussion.

Table 3. B3LYP/6-31G Estimates of the Polaron Binding Energies (meV), Obtained from eq 40 as $E_{pol} = 1/2\lambda_{reorg}$, Related to Electron Transfer (ET) and Hole Transfer (HT) for the Compounds Shown in Figure 14**

molecule	E_{pol} (ET)	E_{pol} (HT)	molecule	E_{pol} (ET)	E_{pol} (HT)
1	129	93	**9**	81	48
2	100	69	**10**	80	47
3	80	57	**11**	119	59
4	66	49	**12**	107	74
5	150	83	**13**	162	175
6	128	54	**14**	147	163
7	106	53	**15**	135	154
8	98	50	**16**	119	140

tion; in addition, no assumption is made regarding the normal-mode coordinates of the two states, the only limitation being the use of the harmonic approximation. In the case of oligoacenes and their derivatives, whose radical-cation and radical-anion ground states are well described by the one-electron approximation, both models yield similar couplings. As an illustrative example, the results obtained for naphthalene are compared in Figure 13.[153]

When only the total relaxation (polaron) energies are of interest, $\lambda_{rel}^{(2)}$ and $\lambda_{rel}^{(1)}$ can be calculated directly from the adiabatic potential energy surfaces (see Figure 12) as[4]

$$\lambda_{rel}^{(1)} = E^{(1)}(M) - E^{(0)}(M) \tag{41}$$

$$\lambda_{rel}^{(2)} = E^{(1)}(M^{+\bullet}) - E^{(0)}(M^{+\bullet}) \tag{42}$$

Here, $E^{(0)}(M)$ and $E^{(0)}(M^{+\bullet})$ are the ground-state energy of the neutral state and the energy of the charged molecular state, respectively, $E^{(1)}(M)$ is the energy of the neutral molecule at the optimal ion geometry, and $E^{(1)}(M^{+\bullet})$ is the energy of the ion state at the optimal geometry of the neutral molecule.

Table 3 collects the DFT estimates of the polaron binding energies E_{pol}(HT) and E_{pol}(ET) associated with hole- and electron-transport processes, respectively, in the series of fused polycyclic benzene-thiophene oligomers illustrated in Figure 14. These molecules are of interest for application in organic electronics.[123,193,194,198,199] In oligoacenes and acene-dithiophenes, the electron–vibration and hole–vibration interactions show similar patterns. In both series, we find that (i) the overall hole–vibration coupling is significantly
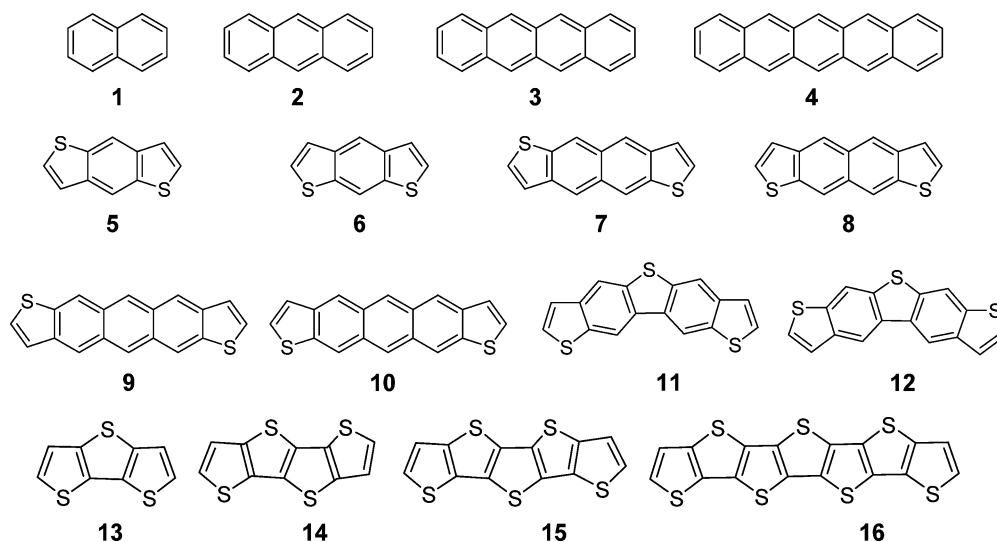
Figure 14. Molecular structure of benzene and/or thiophene fused-ring oligomers: naphthalene (**1**), anthracene (**2**), tetracene (**3**), pentacene (**4**), benzo[1,2-*b*:4,5-*b'*]dithiophene (**5**), benzo[1,2-*b*:5,4-*b'*]dithiophene (**6**), naphtho[2,3-*b*:6,7-*b'*]dithiophene (**7**), naphtho[2,3-*b*:7,6-*b'*]-dithiophene (**8**), anthra[2,3-*b*:7,8-*b'*]dithiophene (**9**), anthra[2,3-*b*:8,7-*b'*]dithiophene (**10**), thieno[2,3-*f*:5,4-*f'*]bis[1]benzothiophene (**11**), thieno-[3,2-*f*:4,5-*f'*]bis[1]benzothiophene (**12**), trithienoacene (**13**), tetrathienoacene (**14**), pentathienoacene (**15**), heptathienoacene (**16**).
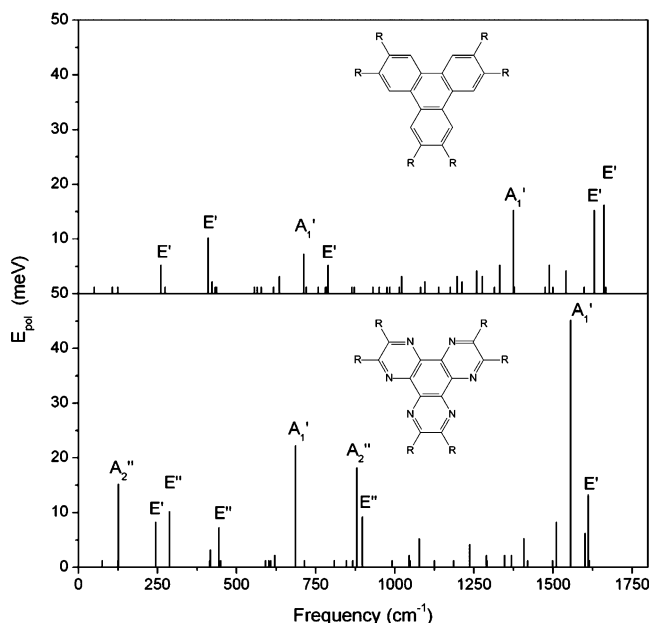
Figure 15. Contribution of the vibrational modes of the triphenylene and hexaazatriphenylene molecules to the polaron binding energy, as calculated at the unrestricted B3LYP/6-31G** level.

smaller than the electron−vibration coupling; (ii) the main contribution to the polaron binding energies E_{pol}(HT) and E_{pol}(ET) comes from high-energy vibrations; and (iii) the electrons interact more strongly than holes with low-energy vibrations.

When, in addition to the terminal rings as in acene-dithiophenes, other benzene rings are also replaced with thiophene rings, these trends no longer hold. For instance, in going from anthradithiophene to thienobisbenzothiophene, the interaction of holes with low-frequency vibrations becomes significant and is larger than the corresponding electron−vibration interaction (see Figure 15). The same pattern is true in oligothienoacenes that consist of fused thiophene rings; in addition, in these compounds, E_{pol}(HT) becomes larger than E_{pol}(ET).[153,193,198,199,201,202]

We note that the neutral, radical-cation, and radical-anion ground states of all systems shown in Figure 14 are orbitally nondegenerate. As a result, according to group theory, only totally symmetric vibrations contribute to the relaxation energy. The situation quickly becomes more complex when the molecules possess a D_3 or higher symmetry. This is the case, for instance, in discotic systems such as triphenylenes and hexabenzocoronenes. The 3-fold symmetry of the conjugated discs often introduces a double degeneracy of the frontier electronic levels. For D_3 symmetry, the addition or removal of one electron from such degenerate levels leads to a degenerate ^{2}E electronic ground state which makes the D_3 configuration of the charged system unstable. As a consequence, new vibronic channels due to Jahn−Teller and/or pseudo-Jahn−Teller interactions open up. Our recent work[116] shows that the electron−vibration interactions in triphenylene derivatives can be significantly affected by minor chemical changes; we found that the overall hole-polaron binding energy in triphenylene (E_{pol} = 90 meV) is nearly doubled when introducing six OH groups on the periphery (E_{pol} = 165 meV). In addition, as seen from Figure 16, the nature of the vibronic interactions markedly changes with nitrogen substitutions as, for instance, in hexaazatriphenylene (HAT). The vibronic coupling in triphenylene is dominated by E′ and A₁′ modes. The introduction of the six nitrogen atoms in HAT leads to a significantly different picture: while the interaction with Jahn−Teller (E′) modes remains moderate, the decrease in energy gap between the ground electronic state ^{2}E′ and the lowest excited electronic state ^{2}A₁′, which is calculated when going from triphenylene to HAT, favors in the latter system a strong pseudo-Jahn−Teller (interstate) coupling of these two electronic states with A₂″ and E″ modes. A systematic study of the impact of these Jahn−Teller and pseudo-Jahn−Teller interactions on the transport properties in discotic systems is still to be performed.

The DFT calculations we carried out on rigid macrocyclic systems such as oligoacenes show that the two components $\lambda_{rel}^{(2)}$ and $\lambda_{rel}^{(1)}$ of the total reorganization energy (see eq 39) are nearly identical. However, the situation is different in oligothiophenes where these two terms differ significantly; see Table 4. This is a consequence of the backbone flexibility present in oligothiophenes as a result of inter-ring torsional
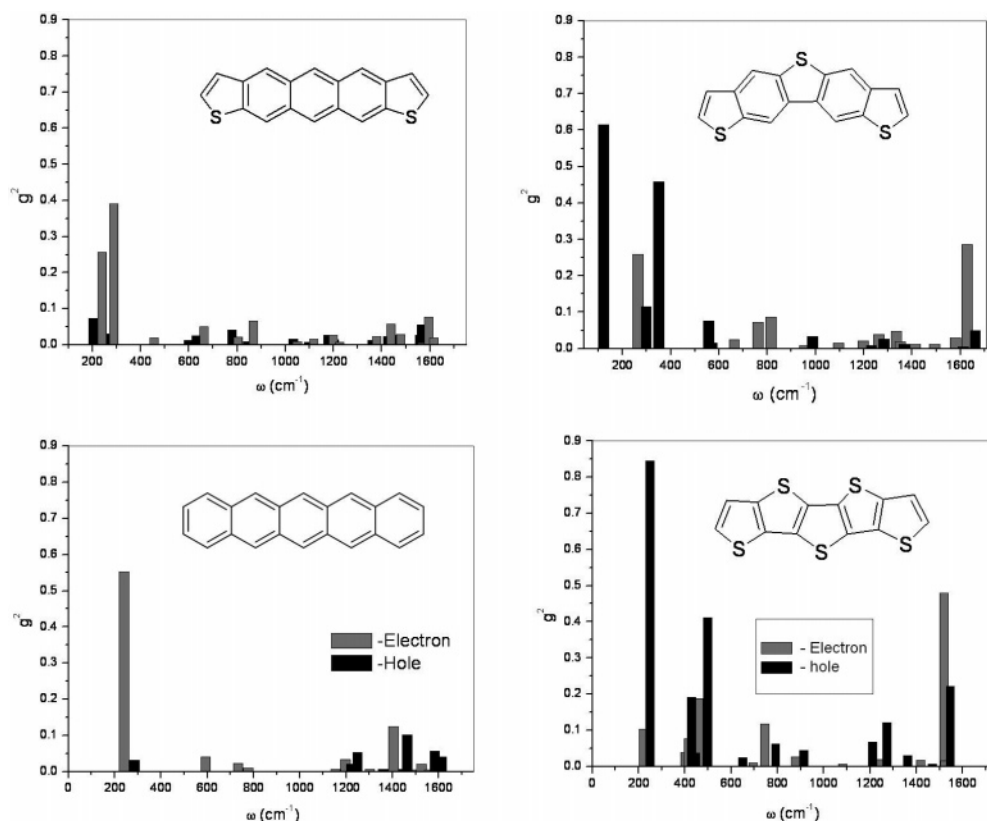
Figure 16. B3LYP/6-31G**-calculated electron− and hole−vibration couplings for compounds **4**, **10**, **11**, and **15** of Figure **14**.

Table 4. B3LYP/6-31G Estimates of the Relaxation Energies Obtained from eqs 41 and 42 for the Thiophene Oligomers Tn (with n the Number of Thiophene Rings)**

molecule	$\lambda_{rel}^{(1)}$ (meV)	$\lambda_{rel}^{(2)}$ (meV)
T1	200	204
T2	187	237
T3	162	211
T4	153	192
T5	142	172
T6	136	165
T7	126	147
T8	119	137

motions. When planarity constraints are used, the relaxation energies $\lambda_{rel}^{(2)}$ and $\lambda_{rel}^{(1)}$ nearly coincide.[203] For similar reasons, the addition of flexible phenyl side-groups leads to an increase by 40% of the hole−vibrational coupling when going from tetracene (E_{pol} = 57 meV) to rubrene (E_{pol} = 80 meV).[153] It should be kept in mind, however, that in the solid state such torsional motions can be hindered. For instance, in single crystals, oligothiophenes tend toward a coplanar conformation;[44] this makes the impact of torsional motions on the electron−vibration coupling less important than what is estimated from gas-phase properties.

It is important to mention that the flexibility of the molecular backbone can lead to significant anharmonicity of the adiabatic potential surfaces of the neutral and charged states, and as a result, to marked differences between the force constants of these states. In such situations, the linear electron−phonon coupling model expressed by eq 18 must be extended and include higher-order terms to reach an adequate description of the charge-transport parameters.[192,204]

To obtain an experimental estimate of the hole−vibration couplings and to assess the adequacy of the various theoreti-

cal approaches, we have exploited the fact that the line shape of the lowest gas-phase ultraviolet photoelectron spectroscopy (UPS) band[193,194] is directly related to the geometry relaxation energy $\lambda_{rel}^{(2)}$ (and thus to the polaron binding energy, E_{pol}). In all the systems we studied to date, we found that, among the standard DFT functionals, B3LYP provides the best description of the geometry modifications upon ionization.[200] The excellent agreement between the experimental and simulated UPS spectra using DFT/B3LYP frequencies and hole−vibrational couplings confirms the reliability of DFT/B3LYP estimates.

Overall, the photoelectron spectroscopy data and DFT results show that in organic molecules the intramolecular contributions to the polaron binding energy do not exceed a few tenths of an eV. The smallest E_{pol} (λ_{rel}) energies are found in large, rigid conjugated macrocycles, such as pentacene, fullerenes, phthalocyanines, and discotic molecules where values can be as low as 0.03−0.05 eV.[116,123,153,193−196,198,199,202] An E_{pol} value of 0.05 eV has also been reported in the case of *trans*-polyacetylene.

We now turn to the discussion of the contribution to the polaron binding energy arising from the external (lattice) degrees of freedom. In analogy to the outer reorganization energy involved in electron-transfer processes, these contributions come from the polarization of the surrounding medium. The first model describing this electron−phonon mechanism was worked out by Gosar and Choi[205] and discussed later by several authors.[206−209]

When an electron (hole) is localized on site m, its site energy ϵ_m is modified by the interaction of the excess charge with the multipole moments (both induced and permanent) of the surrounding molecules. Considering only the interactions with the induced dipole moments and assuming an isotropic molecular model, the contribution to ϵ_m due to

electronic polarization is given by

$$\epsilon_m = -\sum_n \frac{\alpha_0 e^2}{2|\mathbf{R}_m - \mathbf{R}_n|^4} \qquad (43)$$

Here, α_0 is the average molecular polarizabillity and the sum over n runs over all molecules in the crystal. The electron–phonon coupling results from the modulation of ϵ_m by lattice vibrations that takes place via the modulation of the distances $\mathbf{R}_{mn} = |\mathbf{R}_m - \mathbf{R}_n|$ between molecules m and n. The change in ϵ_m resulting from the translation of the molecules (acoustic modes) from their equilibrium position is equal to

$$\Delta\epsilon_m = \sum_{n,\beta} \frac{2\alpha_0 e^2 (\mathbf{R}_m - \mathbf{R}_n)_\beta (\mathbf{u}_m - \mathbf{u}_n)_\beta}{\mathbf{R}_{mn}{}^6} \qquad (44)$$

with β varying from 1 to 3. Expanding the displacements in terms of the creation and annihilation operators according to eq 32 and comparing the result with eq 21 leads to the following expression for the coupling constant:[208]

$$g_m^{(A)}(\mathbf{q},j) = \sum_{n,\beta} \frac{2\alpha_0 e^2 (\mathbf{R}_m - \mathbf{R}_n)_\beta \xi_\beta(\mathbf{q},j)}{\mathbf{R}_{mn}{}^6} \left(\frac{1}{2M_\beta \hbar\omega(\mathbf{q},j)^3}\right)^{1/2}$$
$$(e^{i\mathbf{q}\mathbf{R}_m} - e^{i\mathbf{q}\mathbf{R}_n}) \qquad (45)$$

When applying a Debye model for the acoustic phonons, Vilfan estimated[206] that in anthracene the contribution from this interaction to either hole or electron polaron binding energy is about 40 meV.

An alternative estimate of the lattice contribution was obtained by Brovchenko.[210] With an approach based on empirical atom–atom potentials (such an approach is similar to that based on the adiabatic potential energy surfaces used to evaluate the intramolecular relaxation energy), the overall change in polarization energy in anthracene, due to the lattice relaxation after a localized charge is introduced into the crystal, is estimated to be about 15 meV. These calculations also suggest that the contributions to the lattice relaxation due to rotational motions (librations) are negligible. Thus, the few results reported so far in the literature suggest that, in contrast to the case of electron transfer in solution (where the relaxation energy is usually dominated by outer contributions), when considering organic crystals, the intramolecular contributions are expected to be of the same magnitude as, or even larger than, the contributions from the lattice. However, to reach a more conclusive picture requires more rigorous calculations of the polarization-type coupling constants.

3.2.3. Nonlocal Electron–Phonon Coupling

The nonlocal electron–phonon coupling g_{mn}, as mentioned above, is related to the variations in transfer integrals due to modulations in the distances and relative orientations between molecules. In the rigid-body approximation, this mechanism is entirely due to the interactions with the lattice (external) phonons. The impact of acoustic modes on transfer integrals was first discussed by Friedman.[211] As in the case of local coupling, the nonlocal coupling takes place mainly via
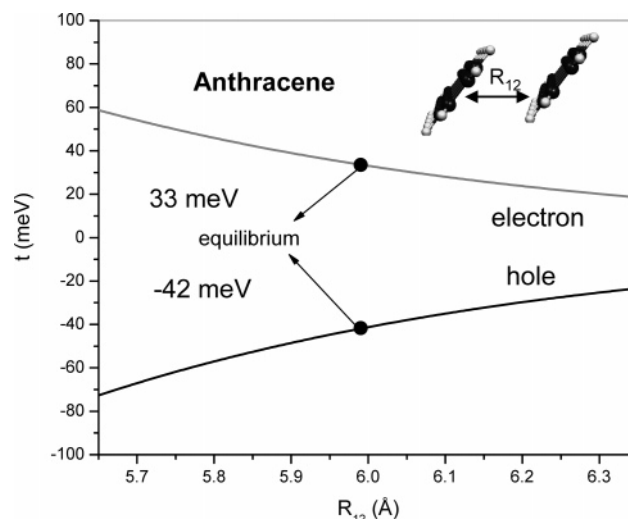
Figure 17. PW91/TZP estimates of the transfer integrals in an anthracene dimer as a function of the intermolecular separation along the short crystal axis.

Table 5. Nonlocal Hole-Phonon Coupling Energies E^{nl} in Oligoacenes (meV) for the a, b, and d (diagonal in the *ab* Plane) Directions (defined according to Table 1)

	naphthalene[a]	anthracene[a]	tetracene[a]	pentacene[b]
t_a	−12	−12	−7	50
E_a^{nl}	0.4	0.1	0.01	6 (9)
t_b	−46	−48	−71	0
E_b^{nl}	2.7	2.3	0.3	0
t_d	14	2	1	−98 (−73)
E_d^{nl}	0.2	1.3	0.1	5(4)

[a] On the basis of parameters obtained from ref 131. [b] On the basis of parameters obtained from refs 187 and 214.

changes in intermolecular distances $\mathbf{R}_{mn}$; it is defined as the first derivative of the transfer integral t_{mn} with respect to $\mathbf{R}_{mn}$: $(\partial t_{mn}/\partial R_{mn})_0$.[211] Unfortunately, to date, a systematic investigation of electron–phonon coupling constants for acoustic phonons is missing. Our experience in calculating transfer integrals underlines that this interaction can be strong (see section 3.1). For instance, in the equilibrium geometry, the transfer integral between two adjacent anthracene molecules along the short crystal axis, see Figure 17, is calculated to be about 0.041 eV; modifying the equilibrium distance by only 0.05 Å (according to molecular dynamic simulations by Deng and Goddard,[212] the displacements at room temperature are expected to be even larger) leads to a variation in the transfer integral of about 30%.

In crystals with two molecules per unit cell, three optical modes exist arising from the translational motions of the rigid molecules. Near the band center ($\mathbf{q} = 0$), these motions are directly related to changes in intermolecular distances and therefore are expected to play an important role in modulating the transfer matrix elements. The nonlocal coupling constants for this type of phonons have been recently estimated for a few systems.[131,187,213,214] To provide more insight on the strength of this interaction, we evaluated the hole-phonon coupling energy E^{nl} in oligoacenes, by using eq 34 (replacing g_m by g_{mn}) and the parameters given in refs 131, 187, and 214. E^{nl} is the equivalent in the nonlocal case of the polaron binding energy for local electron–phonon interaction. The E^{nl} values together with the corresponding transfer integrals are collected in Table 5.

The data do not show any clear trend, except that the coupling constants in pentacene are larger than in smaller oligoacenes. However, this is likely due to the different levels of theory used to estimate the transfer integrals (INDO on dimer for pentacene[214] and DFT band structure[131] for the other systems); in addition, only the coupling with three libration modes is considered in ref 131, while in ref 214 the coupling with all low-energy optical modes is taken into account. As seen from Table 5, except for the diagonal direction in the *ab* plane, the E^{nl} values do not exceed $5-10\%$ of the respective transfer integrals. Interestingly, the main contribution (99%) to E^{nl} along the short crystal axis in pentacene[214] is due to the lowest three energy phonon modes in the range of $27-70$ cm^{-1}; this range is much larger, $27-200$ cm^{-1}, for the nonlocal coupling along the diagonal direction within the *ab* plane. This trend is in line with recent results reported by Troisi and Orlandi for pentacene and anthracene using an approach that combines INDO calculations for the transfer integrals with molecular dynamics simulations for the crystal lattice.[158] These authors show that the variations in transfer integrals due to thermal fluctuations of the lattice are of the same order of magnitude as the corresponding average values. This is a clear indication that the nonlocal electron−phonon coupling is significant. Evidence of strong dependence of the transfer integral on the intermolecular motion has been found experimentally in many organic dimers.[167,169,202,215] Thus, an important conclusion we can draw at this stage is that in organic materials (at least in crystalline systems) the nonlocal electron−phonon coupling appears to be an important interaction and should be included in charge-transport models. However, we emphasize that the calculations of the vibrational couplings with all modes, at a high level of theory and over a much larger range of systems, is still required to provide a better understanding of the nonlocal electron−phonon interactions and their impact on charge transport. In particular, even though the interactions with acoustic modes were the first to be considered, the actual strength of acoustic-like nonlocal interactions is not well-established yet.

4. Overview of the Main Charge-Transport Mechanisms

The study of electron and hole transport in organic materials has a long history going back 60 years[216−218] when the semiconducting nature of organic crystals, their photoconductivity, and electron and hole mobilities were first studied in these systems.[7,8,219−225] In the 1960s, early theoretical work was done by LeBlanc[8,221] and the Chicago group.[226−229] It was clear from the beginning that the purity and molecular order in these crystals were of primary concern for the semiconducting properties, and much work was done to improve these properties.[33,230−234] By the 1970s, the groups at Xerox, Kodak, IBM, and others were investigating transport in highly purified crystals as a function of temperature.[103,235−239] It is worth stressing that Karl at Stuttgart spent 40 years purifying and growing crystals of the simple aromatic hydrocarbons so that the intrinsic properties can be understood.[6] The theoretical work of Kenkre and co-workers[240−243] to describe the electron−phonon interactions that can relate to the observations in highly purified naphthalene and other crystals should also be mentioned. In the mid 1970s, the theoretical description of hopping transport in disordered materials leading to dispersive transport was laid out by Scher and Lax[99] and

Scher and Montroll,[244] using the continuous time random walk (CTRW) model and was later simulated by Bässler and co-workers.[245−247] It was shown to agree with experiments of Bässler and of Haarer,[248,249] who measured transport over many orders of magnitude in time.

For an extensive review of all of this work, see the monographs by Pope and Swenberg,[38] Silinsh and Capek,[117] and the earlier volumes in the series *Physics and Chemistry of the Organic Solid State* edited by Fox.[250] The polaronic and disorder charge-transport mechanisms have been also discussed in detail in several reviews and textbooks.[251−254] Here, we simply outline the main characteristics of the most popular models.

4.1. Polaron Models

The most detailed transport theories are those based on elaborations of the 1D Holstein molecular model. Phenomenological theories, including band theory[255] and the polaron effective mass approach,[117] have been successfully applied in a number of instances. However, these models are limited in scope and restricted to specific ranges of microscopic parameters and temperatures. A more general understanding is provided by microscopic theories that are valid for arbitrary strengths of electronic coupling and local electron−phonon interactions and over the full range of temperatures (derived, for instance, from a density matrix approach,[228] a generalized master equation approach,[242] or more recently a dynamical mean-field theory[256]). According to general and perturbative microscopic models,[38,126,252,253,257] the total mobility can be expressed to a good approximation as a sum of two contributions:

$$\mu = \mu_{\text{tun}} + \mu_{\text{hop}} \qquad (46)$$

Here, the first term is due to electron tunneling (coherent electron transfer) and dominates transport at low temperatures; the second term is related to hopping motion (incoherent electron transfer) and becomes dominant at higher temperatures. The relative contributions of each mechanism depend, however, on the actual values of the microscopic parameters (electron−phonon coupling, electronic and phonon bandwidths, and phonon energy). Illustrative examples of the temperature dependence of the mobility for large ($g^2 \gg 1$) and weak ($g^2 \ll 1$) electron−phonon couplings are schematically depicted in Figure 18. In the case of weak local electron−phonon couplings ($g^2 \ll 1$), the mobility is dominated by tunneling and displays a bandlike temperature dependence ($\mu \sim T^{-n}$, where $n > 0$) in the whole range of temperatures.[228] For intermediate ($g^2 \leq 1$) couplings, the mobility is bandlike at low temperatures; however, due to a significant increase in hopping contributions, it exhibits a weaker temperature dependence at high temperatures. For strong local couplings ($g^2 \gg 1$), three distinct temperature regimes occur; see Figure 18: (i) at low temperatures ($T \ll T_1$), the mobility is bandlike; (ii) as temperature increases, the hopping term starts to dominate, and the mobility exhibits a crossover from coherent transport to an incoherent, temperature-activated transport; (iii) if the system can reach very high temperatures ($T > T_2$) at which the thermal energy becomes large enough to dissociate the polaron, the residual electron is scattered by thermal phonons and as a result the mobility decreases again with temperature. The crossover temperatures T_1 and T_2 are defined by the combination of microscopic parameters; depending on the actual values of
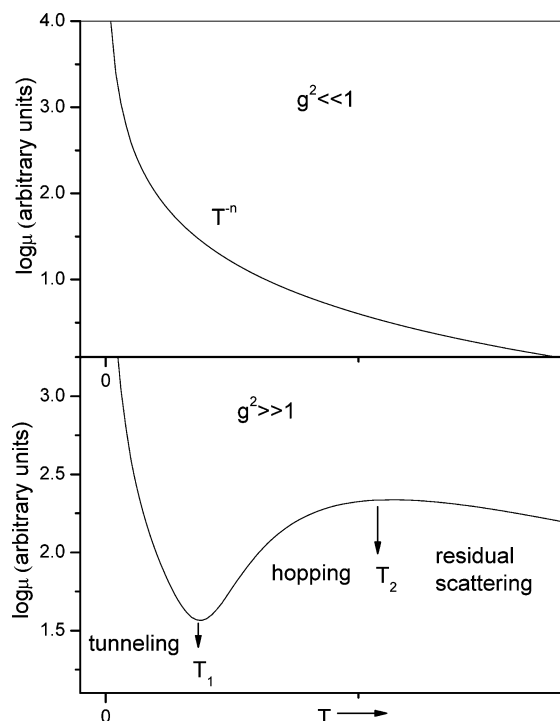
Figure 18. Temperature dependence of the mobility predicted by Holstein polaron model for the limiting cases of strong and weak electron−phonon couplings.

T_1 and T_2, only one or two transport regimes might be experimentally accessible for a particular system.

A significant insight into polaron transport has been obtained from the analytical results (vide infra) derived by Holstein in his seminal work.[125,126] Although these results are based on perturbation theory and limited to the case of very narrow electronic bands (small transfer integrals), they are still extensively used in the literature for qualitative interpretations of experimental data and as a benchmark for new theoretical models. We first consider the hopping mechanism. The hopping mobility, μ_{hop}, can be obtained from eq 2. According to this equation, μ_{hop} is defined by the diffusion coefficient, D; in a 1D system, D is given by $D = a^2\kappa_{ET}$; here, a denotes the spacing between molecules and κ_{ET} is the hopping (electron transfer) rate between adjacent sites. In the framework of small polaron theory, in the case of electron−phonon interactions with an optical phonon of energy $\hbar\omega_0$ and characterized by a coupling constant g (according to eq 34, the polaron binding energy is in this case equal to $E_{pol} = \hbar\omega_0 g^2$), the hopping rate is given by[126]

$$\kappa_{ET} = \frac{t^2}{\hbar^2\omega_0}\left[\frac{\pi}{g^2\,\mathrm{csch}\left(\dfrac{\hbar\omega_0}{2k_BT}\right)}\right]^{1/2}\exp[-2g^2\tanh(\hbar\omega_0/4k_BT)] \tag{47}$$

It follows from eq 47 that in the classical limit for which $\hbar\omega_0 \ll k_BT$, κ_{ET} obeys a standard Arrhenius-type law:

$$\kappa_{ET} = \frac{t^2}{\hbar}\left[\frac{\pi}{2E_{pol}k_BT}\right]^{1/2}\exp(-E_{pol}/2k_BT) \tag{48}$$

When taking into account that $E_{pol} = \lambda_{reorg}/2$, one finds that eq 48 is identical to the classical Marcus equation[141] for electron-transfer rate. Using eqs 2, 47, and 48, we obtain

eqs 49 and 50 for the general and classical limit cases, respectively:

$$\mu_{hop} = \frac{ea^2t^2}{k_BT\hbar^2\omega_0}\left[\frac{\pi}{g^2\,\mathrm{csch}(\hbar\omega_0/2k_BT)}\right]^{1/2}$$
$$\exp\left[-2g^2\tanh\left(\frac{\hbar\omega_0}{4k_BT}\right)\right] \tag{49}$$

$$\mu_{hop} = \frac{ea^2t^2}{k_BT\hbar}\left[\frac{\pi}{2E_{pol}k_BT}\right]^{1/2}\exp(-E_{pol}/2k_BT) \tag{50}$$

At very high temperatures, $E_{pol} \ll 2k_BT$ and eq 50 yields a $T^{-3/2}$ dependence of the mobility in agreement with non-perturbative microscopic theories.[228,242,256,258] This illustrates the crossover from the temperature-activated regime to the residual scattering regime.

We now turn to the discussion of μ_{tun}. In the case of wide conduction bands, according to band theory, the drift mobility is given by $\mu_{tun} = e\tau/m_{eff}$, where τ is the mean relaxation time of the band states (related to the mean free path of the charges), and m_{eff} is the effective mass of the charge carriers (in 1D systems, $\mu_{eff} = \hbar^2/2ta^2$). In this case, the charge moves coherently in a wavelike manner but is scattered (relaxed) by phonons from one momentum state to another. This scattering causes the wavelike nature to change into a diffusive process.

In the narrow band limit, however, all band states are equally populated; as a result, the coherent part of the mobility is given by[126]

$$\mu_{tun} = \frac{2ea^2}{k_BT}\frac{\tau(T)}{\hbar^2}t^2(T) \tag{51}$$

with

$$t(T) = t\exp\{-g^2\coth(\hbar\omega_0/2k_BT)\} \tag{52}$$

A formal analysis shows that the relaxation time $\tau(T)$ of the band states is equal to that of the localized states; therefore, in the lowest-order approximation, $\tau(T)$ is defined by the hopping rate κ_{ET} since $1/\tau(T) = 2\kappa_{ET}$ (a factor of 2 appears since in a 1D model there are two neighbors to which an electron can hop). By inserting eq 47 into eq 51, we obtain

$$\mu_{tun} = \frac{ea^2\omega_0}{k_BT}\left[\frac{g^2\,\mathrm{csch}\left(\dfrac{\hbar\omega_0}{2k_BT}\right)}{\pi}\right]^{1/2}$$
$$\exp(-2g^2\,\mathrm{csch}(\hbar\omega_0/2k_BT)) \tag{53}$$

Note that, because of the assumptions that the band is narrow and the temperature is larger than the electronic bandwidth (as well as other assumptions on the width of the phonon band), the expression does not depend on t. Equation 53 is usually used to discuss the coherent part of the mobility at low temperatures. We note, however, that since it was derived by assuming a narrow band limit, its application is restricted to temperatures such that $k_BT > 4t(T)$.[259] An illustrative example of the temperature dependence of μ_{hop} and μ_{tun}, as obtained from eqs 49 and 53, respectively, is shown in Figure 19.

An important feature of the small polaron theory, which provides the origin of the bandlike to hopping crossover, is
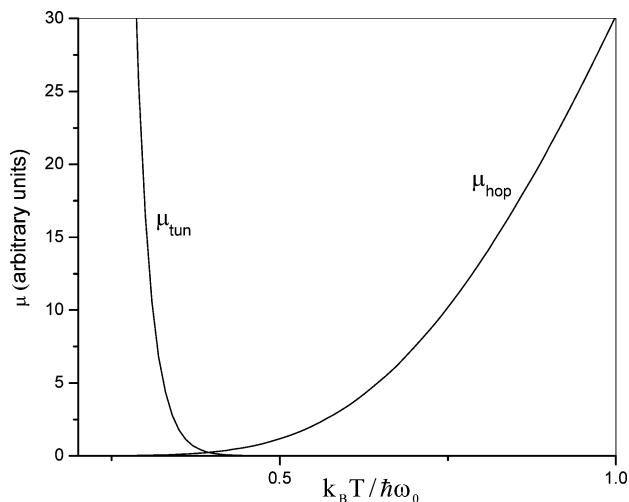
Figure 19. Temperature dependence of the tunnel and hopping contributions to mobility, using the parameters $g^2 = 10$ and $t = \hbar\omega_0$

given by eq 52: the electron−phonon interaction is seen to reduce the transfer integral (bandwidth). The band narrowing is temperature dependent with the polaron band narrower at higher temperatures. Thus, the polaron mass is larger at higher temperatures, thereby reducing the bandlike mobility. Since the hopping contribution increases with temperature, a crossover from one regime to the other is predicted. Evidence for band narrowing with temperature has been recently reported by Koch et al. for a pentacene thin film on graphite.[168] Angle-resolved and energy-dependent ultraviolet photoelectron spectroscopy measurements show that the valence bandwidth along the pentacene (100) direction decreases from 240 meV at 120 K to 190 meV at room temperature.

Interestingly, a direct application of eq 52 to pentacene crystals using the DFT estimates for the parameters corresponding to *intra*-molecular polaron coupling fails to explain this temperature effect because of the high energy of the *intra*-molecular vibrations. However, the experimental data can be explained very well by assuming an electron−phonon interaction with a low-energy mode in the range of 10−20 meV. The fitting then yields a polaron binding energy of 6−30 meV, which is in the range expected for intermolecular (external) modes. Using a simple 1D model, we estimate a value of ∼70−75 meV for the transfer integral in pentacene; this value is in good agreement with the results of the DFT calculations presented in section 3.

Despite its qualitative agreement with experiment, transport theories based solely on the original Holstein molecular model cannot fully describe the charge-transport mechanisms in organic materials. The fact that in organic crystals the variations in transfer integral with acoustic and optical phonons, as discussed in previous sections, can be of the same order of magnitude as the value of the transfer integral itself,[158] demonstrates that more general models need to be considered.

An attempt to extend the microscopic transport theory for the case where both local and nonlocal couplings are operative was made by Munn and Silbey.[127,128] It was found that nonlocal coupling increases the polaron binding energy and impacts the bandwidth. In contrast to local coupling which always narrows the band, nonlocal coupling, depending on the actual values of the microscopic parameters, can change the band shape in a way that introduces new minima

and can lead to band broadening. It was also shown that in general nonlocal coupling increases scattering, thereby reducing the tunneling (bandlike or coherent) contribution to the mobility.

A microscopic model based on the Holstein model generalized to higher dimensions and utilizing the generalized master equation approach has been applied by Kenkre et al.[242] to explain the temperature dependence and anisotropy of charge transport in naphthalene. This model was found to reproduce the experimental mobilities very well. However, the fitting was based on directionally dependent local electron−phonon interactions and on values of electronic coupling of 2 meV that are significantly smaller than the DFT and INDO estimates.

A microscopic charge transport theory based on a Holstein-Peierls-type Hamiltonian has been recently presented by Bobbert and co-workers.[131,260] Using this model and microscopic parameters derived from ab initio calculations, the authors were able to reproduce the experimental data in naphthalene.[260] The model, however, only accounts for the intermolecular optical modes; thus, it neglects the contributions from *intra*-molecular vibrations and, more importantly, the coupling to acoustic modes that appears to play a significant role in charge transport. The Bobbert approach, as well as the Munn and Silbey approach, are based on a nonlocal-type canonical transformation (an extension of the small polaron approach) while omitting specific terms. The consequences of these approximations and, therefore, the range of validity of both models are still an open question, although both give qualitative results in agreement with experiment.

Recently, Hultell and Stafström[261] and Troisi and Orlandi[262] have discussed the problem of charge transport in organic semiconductors by using numerical solutions of the time-dependent Schrödinger equation and treating the vibrations classically. Only local coupling was considered by the former authors and only nonlocal coupling was considered by the latter. From the discussion of the microscopic parameters given in the previous section, it is clear, however, that *both* local and nonlocal interactions should be taken into account. A complete understanding can be obtained only from a microscopic theory that treats the whole Hamiltonian self-consistently. A full knowledge of the microscopic parameters is the first step toward the development of a comprehensive approach. In addition, because the vibrations are treated classically, this theory can only be valid for the range of temperatures where the thermal energy is larger than the average vibrational frequency.

4.2. Disorder Models

So far, we have considered the situation where chemical and physical defects are absent and charge transport is limited by the dynamic disorder arising from electron−phonon coupling. We now provide a description of charge transport in the presence of static disorder; this transport mechanism is expected to be operative in many organic materials since they usually present a highly amorphous character. Disorder tends to localize the band states found in highly ordered materials. In 3D materials, when disorder is weak, only the states at the band edge are truly localized. Increasing the amount of disorder localizes more and more of the states in the band, until all states become localized in the case of strong disorder. Transport then operates in the hopping regime with charges jumping between interacting molecules.

In the case of amorphous conjugated polymer films, we note that diagonal disorder is induced both by electrostatic effects and a distribution in effective conjugation lengths while off-diagonal disorder comes from a distribution in the relative positions/separations between adjacent units.

While we documented earlier numerous instances where the transfer integrals and electron−phonon couplings can be derived from first principles, the theoretical studies performed on disordered materials have often been purely phenomenological in nature. The charge-transfer rates between interacting molecules are typically evaluated on the basis of effective parameters fitted to experimental data. The simplest way to describe charge transport in organic disordered materials, as was shown by Bässler and co-workers, is via Monte Carlo (MC) simulations.[25] There are two essential inputs in this approach, the charge hopping rates between sites and the density of hopping states.

Two main models exist for the hopping rates usually considered in the literature. The first model, used especially in the early studies, is that of Miller-Abrahams originally developed to describe charge transport in doped inorganic semiconductors.[263] In the Miller-Abrahams formalism, the hopping rate κ_{ij} from site i to site j is expressed as

$$\kappa_{ij} = \nu \exp(-2\gamma R_{ij}) \begin{cases} \exp\left(-\dfrac{\epsilon_j - \epsilon_i}{k_{\mathrm{B}}T}\right) & \epsilon_j > \epsilon_i \\ 1 & \epsilon_j < \epsilon_i \end{cases} \quad (54)$$

Here, ν denotes the attempt hopping frequency; R_{ij} is the separation between sites i and j; γ is the overlap factor; and ϵ_i and ϵ_j are the site energies. The first exponential term accounts for the decrease in electronic coupling with distance; note, however, that it does not incorporate the sensitivity of the electronic coupling on the relative orientations of the interacting molecules. The last term is a Boltzmann factor for a jump upward in energy and is equal to 1 for a jump downward in energy. In the presence of an electric field, an additional term, expressed as $[-e\vec{r}\vec{F}]$, is introduced in the energetic balance (top right term in eq 54), with $\vec{r}$ the vector connecting the centers of the two sites and $\vec{F}$ the electric field vector. Thus, in the Miller-Abrahams formalism, downward jumps are not accelerated by the electric field and are assumed to always occur whatever the extent of the site energy difference (i.e., this assumes that there is always a channel to accept the energy difference).

The second model for hopping rates is the Marcus expression for semi-classical electron-transfer rates.[141] This expression represents a generalization of eq 48 to the case of nonequivalent sites:

$$\kappa_{ij} = \frac{t^2}{\hbar}\left[\frac{\pi}{k_{\mathrm{B}}T\lambda_{\mathrm{reorg}}}\right]^{1/2} \exp\left[-\frac{(\lambda_{\mathrm{reorg}} + \epsilon_j - \epsilon_i)^2}{4\lambda_{\mathrm{reorg}}k_{\mathrm{B}}T}\right] \quad (55)$$

Off-diagonal disorder, which arises from fluctuations in electronic couplings, can be introduced as in the Miller-Abrahams approach by making the assumption of an exponential dependence for t: $t = t_0 \exp(-\gamma R_{ij})$. A major implication of the Marcus expression, which has been at the heart of its success in describing electron-transfer reactions, is that, because of the vibrational degrees of freedom, the transfer rate does not keep continuously increasing with increasing driving force, $\Delta G° = \epsilon_j - \epsilon_i$ (note that this definition neglects the entropy contribution). For a given λ value and considering a negative driving force, the transfer

rate first increases with the magnitude of $\Delta G°$ (this is referred to as the normal region); it reaches a maximum when $|\Delta G°| = \lambda$; importantly, it decreases when $|\Delta G°| > \lambda$ (inverted region). The inverted region is totally absent in the Miller-Abrahams formalism.

We note that both Marcus and Miller-Abrahams expressions can be derived as two limiting cases from a more general expression obtained by means of time-dependent perturbation theory for the case of weak electronic coupling. The Miller-Abrahams equation is valid for weak electron−phonon (vibration) coupling and low temperatures. The electron hops upward or downward in energy in this approximation are characterized by absorption or emission of a single phonon, respectively, that compensates for the energy difference $\epsilon_j - \epsilon_i$. It is then clear that the Miller-Abrahams model only applies for $[\epsilon_j - \epsilon_i]$ values that do not exceed the maximum (Debye) energy of the acoustical phonons and the energy of the optical phonons effectively coupled to the electron-transfer reaction; in the case of oligoacenes, for instance, the characteristic energy of these optical phonons is on the order of 0.15 eV. Since the phonon absorption process depends on the availability of phonons in the system, the upward hops are temperature activated. The downward hops, as expected, are temperature independent. In contrast to the Miller-Abrahams model, the Marcus expression is valid for large electron−phonon (vibration) couplings and high temperatures.

Disorder is introduced by attributing to each site a random energy ϵ picked from a distribution of states, usually assumed to be of Gaussian shape:

$$Q(\epsilon) = \frac{1}{\sqrt{2\pi\sigma^2}}\exp\left(-\frac{\epsilon^2}{2\sigma^2}\right) \quad (56)$$

where σ is the standard deviation of the distribution. There is no direct experimental proof for using a Gaussian shape; the only justification comes from the shape of the absorption bands in disordered organic materials. The standard deviation for the density of (localized) states (DOS) is typically found to be around 0.1 eV. A consequence of the energetic disorder is that the carriers tend to relax into the tail of the DOS distribution during the simulation. After equilibration, the mean energy of a charge carrier at zero electric field, $\langle \epsilon_\infty \rangle$, shifts to an energy equal to $-\sigma^2/kT$. To consider local variations in intersite distances as well as the non-isotropic nature of the electronic coupling, the overlap factor γ in eq 54 can also be assumed to be randomly distributed. A significant improvement in the description of positional disorder can be found in an approach where the transfer integrals between each pair of interacting molecules are calculated at the quantum-chemical level and then injected into Monte Carlo simulations, as described recently.[264] However, this requires the knowledge of the microscopic morphology of the material, which is difficult to assess but can be evaluated for instance from simulations based on effective molecular potentials.

Temperature Dependence. When the mobility is extrapolated at the zero-field limit, the fit of the MC results leads to the following expression:

$$\mu(T) = \mu_0 \exp\left[-\left(\frac{2\sigma}{3k_{\mathrm{B}}T}\right)^2\right] = \mu_0 \exp\left[-\left(\frac{T_0}{T}\right)^2\right] \quad (57)$$

with σ representing the width of the diagonal disorder. Since

the temperature helps in overcoming the barriers introduced by the energetic disorder in the system and its impact is not included in the overlap factor γ in eq 54, the temperature evolution here only depends on the amplitude of σ. This expression deviates from an Arrhenius-like law (see section 2.3), although both expressions do generally fit the experimental data well, as a result of the limited range of temperatures available.

Field Dependence. The impact of an external electric field is to lower the barrier for upward energy hops; this allows the charges to leave the states in the tail of the DOS, that would otherwise act as traps. In the presence of energetic disorder only, the Monte Carlo results generally yield a Poole-Frenkel behavior (i.e., a $F^{1/2}$ dependence with respect to field) for electric fields larger than 10^4-10^5 V/cm, with mobility constant at lower fields. The field dependence becomes more pronounced as the extent of energetic disorder grows. The increase in electric field amplitude is also accompanied by an increased diffusion constant. A deviation from Einstein's relation is, however, suggested by Monte Carlo simulations at high electric fields and with large energetic disorder. Tessler and co-workers have also pointed out that Einstein's relation should be generalized in the presence of a high density of charge carriers. Interestingly, mobility drops with increasing field at low energetic disorder; this can be explained within the Miller-Abrahams formalism by a saturation of the velocity distribution (without having to refer to a Marcus inverted region).

While not involved in the temperature dependence, the positional (off-diagonal) disorder plays a key role in defining the field dependence of the mobility. From the results of Monte Carlo simulations, the general behavior of the mobility as a function of both temperature and electric field in the presence of diagonal and off-diagonal disorder is given by

$$\mu(\tilde{\sigma},\Sigma,F) = \mu_0 \exp\left[-\left(\frac{2}{3}\tilde{\sigma}\right)^2\right] \times$$

$$\begin{cases} \exp[C(\tilde{\sigma}^2 - \Sigma^2)F^{1/2}] & \Sigma \geq 1.5 \\ \exp[C(\tilde{\sigma}^2 - 2.25)F^{1/2}] & \Sigma < 1.5 \end{cases} \quad (58)$$

where $\tilde{\sigma} = \sigma/kT$, Σ is the standard deviation associated with the non-diagonal disorder, and C is a numerical constant. We recover the expression given in eq 57 when $F = 0$. Positional disorder and electric field are linked since the higher directionality imposed by the field prevents the charge from being able to avoid regions where sites are weakly electronically coupled. If the extent of positional disorder (Σ) is larger than the width of energetic disorder (σ), eq 58 points to a mobility decrease when the electric field is increased, an observation that has been reported for a few systems.[109]

The results of Monte Carlo simulations by Bässler and co-workers[25,265] show that the mobility obeys a Poole-Frenkel behavior over an extended range of electric fields, generally above 10^4-10^5 V/cm. However, such results do not account for the fact that a Poole-Frenkel behavior is also observed in many cases at lower electric fields. A main limitation of the Monte Carlo scheme described above is that the energies are distributed totally randomly over the sites. In some instances, using a fully random distribution appears to be too severe an approximation, which has motivated the development of models incorporating a *correlated* energetic disorder.[88–91,265–269] The need for correlated models has been illustrated, for instance, in systems where the molecules have

a permanent dipole;[90] in such a case, the energy distribution has a well-defined profile governed to first order by the interactions between the charge and the induced and permanent dipoles of the neighboring molecules.

The models described above deal with the temperature and field dependences of the mobility; they do not account for the dependence on charge carrier density, whose role has been evidenced experimentally; see section 2.3.[16] The mobility dependence on charge density is not simply related to Coulomb repulsion among the charge carriers; rather, it reflects the fact that, for large carrier concentrations, only a fraction of the carriers is necessary to populate the tail of the density of states (traps), which allows the other carriers to be more mobile. Various models treating the impact of charge-carrier density have been recently reviewed by Coehoorn et al.[270]

5. Synopsis

In this review, we have discussed the major advances that have recently been achieved in the description of the parameters impacting charge transport in organic semiconductors. Once again, the picture emerging in organic semiconductors appears to be more complex than in conventional inorganic semiconductors; this was the case already when comparing the electronic structure of these materials: while inorganic semiconductors can usually be well described via one-electron (band structure) approaches, organic semiconductors often require a treatment that takes both electron–electron and electron–phonon interactions into account.

In the case of transport, we emphasized in sections 3 and 4 some of the shortcomings of the current models used to depict organic semiconductors and the paths to be followed to achieve significant improvements. An important element is that it has become clear that organic semiconductors require that both local and nonlocal electron–phonon couplings be considered. Thus, we can conclude that a comprehensive understanding will come from the development of models allowing the calculations of the vibrational couplings: (i) with all modes, optical as well as acoustical since the actual strength of acoustic-type nonlocal interactions is not well-established yet; (ii) at a high level of theory; and (iii) over a much larger range of systems than those that have been examined to date.

We hope that this review will provide the impetus for these calculations to be undertaken.

6. Acknowledgments

7. Note Added after Print Publication

Due to a production error, there were misplaced parentheses in eqs 54 and 58 in the version posted on the Web March 23, 2007 (ASAP) and published in the April 11, 2007 issue (Vol. 107, No. 4, pp 926−952); the correct electronic version of the paper was published on May 1, 2007, and an Addition and Correction appears in the May 9, 2007 issue (Vol. 107, No. 5).

8. References

(1) Su, W. P.; Schrieffer, J. R.; Heeger, A. J. *Phys. Rev. Lett.* **1979**, *42*, 1698.
(2) Bredas, J. L.; Street, G. B. *Acc. Chem. Res.* **1985**, *18*, 309.
(3) Heeger, A. J.; Kivelson, S.; Schrieffer, J. R.; Su, W. P. *Rev. Mod. Phys.* **1988**, *60*, 781.
(4) Bredas, J. L.; Beljonne, D.; Coropceanu, V.; Cornil, J. *Chem. Rev.* **2004**, *104*, 4971.
(5) Zaumseil, J.; Sirringhaus, H. *Chem. Rev.* **2007**, 107, 1296−1323.
(6) Karl, N. *Synth. Met.* **2003**, *133*, 649.
(7) Kepler, R. G. *Phys. Rev.* **1960**, *119*, 1226.
(8) Leblanc, O. H. *J. Chem. Phys.* **1960**, *33*, 626.
(9) Horowitz, G. *Adv. Mater.* **1998**, *10*, 365.
(10) Horowitz, G. *J. Mater. Res.* **2004**, *19*, 1946.
(11) Dodabalapur, A.; Torsi, L.; Katz, H. E. *Science* **1995**, *268*, 270.
(12) Pesavento, P. V.; Chesterfield, R. J.; Newman, C. R.; Frisbie, C. D. *J. Appl. Phys.* **2004**, *96*, 7312.
(13) Goldmann, C.; Haas, S.; Krellner, C.; Pernstich, K. P.; Gundlach, D. J.; Batlogg, B. *J. Appl. Phys.* **2004**, *96*, 2080.
(14) Podzorov, V.; Sysoev, S. E.; Loginova, E.; Pudalov, V. M.; Gershenson, M. E. *Appl. Phys. Lett.* **2003**, *83*, 3504.
(15) Dimitrakopoulos, C. D.; Purushothaman, S.; Kymissis, J.; Callegari, A.; Shaw, J. M. *Science* **1999**, *283*, 822.
(16) Tanase, C.; Meijer, E. J.; Blom, P. W. M.; de Leeuw, D. M. *Phys. Rev. Lett.* **2003**, *91*, 216601.
(17) Stassen, A. F.; de Boer, R. W. I.; Iosad, N. N.; Morpurgo, A. F. *Appl. Phys. Lett.* **2004**, *85*, 3899.
(18) Veres, J.; Ogier, S. D.; Leeming, S. W.; Cupertino, D. C.; Khaffaf, S. M. *Adv. Funct. Mater.* **2003**, *13*, 199.
(19) Kirova, N.; Bussac, M. N. *Phys. Rev. B* **2003**, *68*, 235312.
(20) Houili, H.; Picon, J. D.; Zuppiroli, L.; Bussac, M. N. *J. Appl. Phys.* **2006**, *100*, 023702.
(21) Hulea, I. N.; Fratini, S.; Xie, H.; Mulder, C. L.; Iossad, N. N.; Rastelli, G.; Ciuchi, S.; Morpurgo, A. F. *Nat. Mater.* **2006**, *5*, 982.
(22) Coropceanu, V.; Bredas, J. L. *Nat. Mater.* **2006**, *5*, 929.
(23) Blom, P. W. M.; deJong, M. J. M.; Vleggaar, J. J. M. *Appl. Phys. Lett.* **1996**, *68*, 3308.
(24) Fichou, D. *Handbook of Oligo- and Polythiophenes*; Wiley-VCH: Weinheim: New York, 1999.
(25) Bassler, H. *Phys. Status Solidi B* **1993**, *175*, 15.
(26) Horowitz, G.; Hajlaoui, M. E.; Hajlaoui, R. *J. Appl. Phys.* **2000**, *87*, 4456.
(27) van de Craats, A. M.; Warman, J. M. *Adv. Mater.* **2001**, *13*, 130.
(28) Warman, J. M.; de Haas, M. P.; Dicker, G.; Grozema, F. C.; Piris, J.; Debije, M. G. *Chem. Mater.* **2004**, *16*, 4600.
(29) Prins, P.; Candeias, L. P.; van Breemen, A. J. J. M.; Sweelssen, J.; Herwig, P. T.; Schoo, H. F. M.; Siebbeles, L. D. A. *Adv. Mater.* **2005**, *17*, 718.
(30) Hoofman, R. J. O. M.; de Haas, M. P.; Siebbeles, L. D.; Warman, J. M. *Nature* **1998**, *392*, 54.
(31) Prins, P.; Grozema, F. C.; Schins, J. M.; Savenije, T. J.; Patil, S.; Scherf, U.; Siebbeles, L. D. A. *Phys. Rev. B* **2006**, *73*, 045204.
(32) Jurchescu, O. D.; Baas, J.; Palstra, T. T. M. *Appl. Phys. Lett.* **2004**, *84*, 3061.
(33) Warta, W.; Karl, N. *Phys. Rev. B* **1985**, *32*, 1172.
(34) Podzorov, V.; Pudalov, V. M.; Gershenson, M. E. *Appl. Phys. Lett.* **2003**, *82*, 1739.
(35) Shirota, Y. *J. Mater. Chem.* **2005**, *15*, 75.
(36) Kreouzis, T.; Poplavskyy, D.; Tuladhar, S. M.; Campoy-Quiles, M.; Nelson, J.; Campbell, A. J.; Bradley, D. D. C. *Phys. Rev. B* **2006**, *73*, 235201.
(37) de Boer, R. W. I.; Gershenson, M. E.; Morpurgo, A. F.; Podzorov, V. *Phys. Status Solidi A* **2004**, *201*, 1302.
(38) Pope, M.; Swenberg, C. E.; Pope, M. *Electronic Processes in Organic Crystals and Polymers*, 2nd ed.; Oxford University Press: New York, 1999.
(39) Rutenberg, I. M.; Scherman, O. A.; Grubbs, R. H.; Jiang, W. R.; Garfunkel, E.; Bao, Z. *J. Am. Chem. Soc.* **2004**, *126*, 4062.
(40) Zeis, R.; Besnard, C.; Siegrist, T.; Schlockermann, C.; Chi, X. L.; Kloc, C. *Chem. Mater.* **2006**, *18*, 244.
(41) Sundar, V. C.; Zaumseil, J.; Podzorov, V.; Menard, E.; Willett, R. L.; Someya, T.; Gershenson, M. E.; Rogers, J. A. *Science* **2004**, *303*, 1644.
(42) Podzorov, V.; Menard, E.; Borissov, A.; Kiryukhin, V.; Rogers, J. A.; Gershenson, M. E. *Phys. Rev. Lett.* **2004**, *93*, 086602.
(43) Mattheus, C. C.; de Wijs, G. A.; de Groot, R. A.; Palstra, T. T. M. *J. Am. Chem. Soc.* **2003**, *125*, 6323.
(44) Fichou, D. *J. Mater. Chem.* **2000**, *10*, 571.
(45) Chang, P. C.; Lee, J.; Huang, D.; Subramanian, V.; Murphy, A. R.; Frechet, J. M. J. *Chem. Mater.* **2004**, *16*, 4783.
(46) Fichou, D.; Bachet, B.; Demanze, F.; Billy, I.; Horowitz, G.; Garnier, F. *Adv. Mater.* **1996**, *8*, 500.
(47) Garnier, F.; Hajlaoui, R.; Yassar, A.; Srivastava, P. *Science* **1994**, *265*, 1684.
(48) Sakamoto, Y.; Suzuki, T.; Kobayashi, M.; Gao, Y.; Fukai, Y.; Inoue, Y.; Sato, F.; Tokito, S. *J. Am. Chem. Soc.* **2004**, *126*, 8138.
(49) Yoon, M. H.; Facchetti, A.; Stern, C. E.; Marks, T. J. *J. Am. Chem. Soc.* **2006**, *128*, 5792.
(50) Newman, C. R.; Frisbie, C. D.; da Silva, D. A.; Bredas, J. L.; Ewbank, P. C.; Mann, K. R. *Chem. Mater.* **2004**, *16*, 4436.
(51) Jones, B. A.; Ahrens, M. J.; Yoon, M. H.; Facchetti, A.; Marks, T. J.; Wasielewski, M. R. *Angew. Chem., Int. Ed.* **2004**, *43*, 6363.
(52) Adam, D.; Schuhmacher, P.; Simmerer, J.; Haussling, L.; Siemensmeyer, K.; Etzbach, K. H.; Ringsdorf, H.; Haarer, D. *Nature* **1994**, *371*, 141.
(53) van de Craats, A. M.; Warman, J. M.; Fechtenkotter, A.; Brand, J. D.; Harbison, M. A.; Mullen, K. *Adv. Mater.* **1999**, *11*, 1469.
(54) An, Z. S.; Yu, J. S.; Jones, S. C.; Barlow, S.; Yoo, S.; Domercq, B.; Prins, P.; Siebbeles, L. D. A.; Kippelen, B.; Marder, S. R. *Adv. Mater.* **2005**, *17*, 2580.
(55) Shiyanovskaya, I.; Singer, K. D.; Twieg, R. J.; Sukhomlinova, L.; Gettwert, V. *Phys. Rev. E* **2002**, *65*, 041715.
(56) Funahashi, M.; Hanna, J. *Phys. Rev. Lett.* **1997**, *78*, 2184.
(57) Ducharme, S.; Borsenberger, P. M. Xerographic Photoreceptors and Photorefractive Polymers, July 10−11, 1995, San Diego, CA; Society of Photo-optical Instrumentation Engineers: Bellingham, WA, 1995.
(58) Camerman, A.; Trotter, J. *Proc. R. Soc. London, A* **1964**, *279*, 129.
(59) Ferraris, J.; Cowan, D. O.; Walatka, V.; Perlstein, J. H. *J. Am. Chem. Soc.* **1973**, *95*, 948.
(60) Otsubo, T.; Takimiya, K. *Bull. Chem. Soc. Jpn.* **2004**, *77*, 43.
(61) Rovira, C. *Chem. Rev.* **2004**, *104*, 5289.
(62) Mas-Torrent, M.; Hadley, P.; Bromley, S. T.; Crivillers, N.; Veciana, J.; Rovira, C. *Appl. Phys. Lett.* **2005**, *86*, 012110.
(63) Mas-Torrent, M.; Durkut, M.; Hadley, P.; Ribas, X.; Rovira, C. *J. Am. Chem. Soc.* **2004**, *126*, 984.
(64) Haddon, R. C.; Perel, A. S.; Morris, R. C.; Palstra, T. T. M.; Hebard, A. F.; Fleming, R. M. *Appl. Phys. Lett.* **1995**, *67*, 121.
(65) Frankevich, E.; Maruyama, Y.; Ogata, H.; Achiba, Y.; Kikuchi, K. *Solid State Commun.* **1993**, *88*, 177.
(66) Durkop, T.; Kim, B. M.; Fuhrer, M. S. *J. Phys.: Condens. Matter* **2004**, *16*, R553.
(67) Sirringhaus, H.; Brown, P. J.; Friend, R. H.; Nielsen, M. M.; Bechgaard, K.; Langeveld-Voss, B. M. W.; Spiering, A. J. H.; Janssen, R. A. J.; Meijer, E. W.; Herwig, P.; de Leeuw, D. M. *Nature* **1999**, *401*, 685.
(68) Mcculloch, I.; Heeney, M.; Bailey, C.; Genevicius, K.; Macdonald, I.; Shkunov, M.; Sparrowe, D.; Tierney, S.; Wagner, R.; Zhang, W. M.; Chabinyc, M. L.; Kline, R. J.; Mcgehee, M. D.; Toney, M. F. *Nat. Mater.* **2006**, *5*, 328.
(69) Sirringhaus, H.; Wilson, R. J.; Friend, R. H.; Inbasekaran, M.; Wu, W.; Woo, E. P.; Grell, M.; Bradley, D. D. C. *Appl. Phys. Lett.* **2000**, *77*, 406.
(70) Burroughes, J. H.; Bradley, D. D. C.; Brown, A. R.; Marks, R. N.; Mackay, K.; Friend, R. H.; Burns, P. L.; Holmes, A. B. *Nature* **1990**, *347*, 539.
(71) Friend, R. H.; Gymer, R. W.; Holmes, A. B.; Burroughes, J. H.; Marks, R. N.; Taliani, C.; Bradley, D. D. C.; Dos Santos, D. A.; Bredas, J. L.; Logdlund, M.; Salaneck, W. R. *Nature* **1999**, *397*, 121.
(72) Bernius, M. T.; Inbasekaran, M.; O'Brien, J.; Wu, W. S. *Adv. Mater.* **2000**, *12*, 1737.
(73) Babel, A.; Jenekhe, S. A. *Adv. Mater.* **2002**, *14*, 371.

(74) Bredas, J. L.; Calbert, J. P.; da Silva, D. A.; Cornil, J. *Proc. Natl. Acad. Sci. U.S.A.* **2002**, *99*, 5804.
(75) Cornil, J.; Beljonne, D.; Calbert, J. P.; Bredas, J. L. *Adv. Mater.* **2001**, *13*, 1053.
(76) Kazukauskas, V.; Tzeng, H.; Chen, S. A. *Appl. Phys. Lett.* **2002**, *80*, 2017.
(77) Smits, E. C. P.; Anthopoulos, T. D.; Setayesh, S.; van Veenendaal, E.; Coehoorn, R.; Blom, P. W. M.; de Boer, B.; de Leeuw, D. M. *Phys. Rev. B* **2006**, *73*, 205316.
(78) Chua, L. L.; Zaumseil, J.; Chang, J. F.; Ou, E. C. W.; Ho, P. K. H.; Sirringhaus, H.; Friend, R. H. *Nature* **2005**, *434*, 194.
(79) Lee, J. Y.; Roth, S.; Park, Y. W. *Appl. Phys. Lett.* **2006**, *88*, 252106.
(80) Fritz, S. E.; Martin, S. M.; Frisbie, C. D.; Ward, M. D.; Toney, M. F. *J. Am. Chem. Soc.* **2004**, *126*, 4084.
(81) Valeev, E. F.; Coropceanu, V.; da Silva, D. A.; Salman, S.; Bredas, J. L. *J. Am. Chem. Soc.* **2006**, *128*, 9882.
(82) Sheraw, C. D.; Jackson, T. N.; Eaton, D. L.; Anthony, J. E. *Adv. Mater.* **2003**, *15*, 2009.
(83) Mas-Torrent, M.; Hadley, P.; Bromley, S. T.; Ribas, X.; Tarres, J.; Mas, M.; Molins, E.; Veciana, J.; Rovira, C. *J. Am. Chem. Soc.* **2004**, *126*, 8546.
(84) Gavezzotti, A. *Acc. Chem. Res.* **1994**, *27*, 309.
(85) Beyer, T.; Lewis, T.; Price, S. L. *CrystEngComm* **2001**, *3*, 212.
(86) Kazmaier, P. M.; Hoffmann, R. *J. Am. Chem. Soc.* **1994**, *116*, 9684.
(87) Wurthner, F. *Chem. Commun.* **2004**, 1564.
(88) Dieckmann, A.; Bassler, H.; Borsenberger, P. M. *J. Chem. Phys.* **1993**, *99*, 8136.
(89) Borsenberger, P. M.; Fitzgerald, J. J. *J. Phys. Chem.* **1993**, *97*, 4815.
(90) Dunlap, D. H.; Parris, P. E.; Kenkre, V. M. *Phys. Rev. Lett.* **1996**, *77*, 542.
(91) Novikov, S. V. *J. Polym. Sci., Part B: Polym. Phys.* **2003**, *41*, 2584.
(92) Blom, P. W. M.; deJong, M. J. M.; vanMunster, M. G. *Phys. Rev. B* **1997**, *55*, R656.
(93) Sirringhaus, H. *Adv. Mater.* **2005**, *17*, 2411.
(94) Karl, N.; Kraft, K. H.; Marktanner, J.; Munch, M.; Schatz, F.; Stehle, R.; Uhde, H. M. *J. Vac. Sci. Technol., A* **1999**, *17*, 2318.
(95) Dimitrakopoulos, C. D.; Mascaro, D. J. *IBM J. Res. Develop.* **2001**, *45*, 11.
(96) Lecomber, P. G.; Spear, W. E. *Phys. Rev. Lett.* **1970**, *25*, 509.
(97) Schmidlin, F. W. *Phys. Rev. B* **1977**, *16*, 2362.
(98) Noolandi, J. *Phys. Rev. B* **1977**, *16*, 4474.
(99) Scher, H.; Lax, M. *Phys. Rev. B* **1973**, *7*, 4491.
(100) Horowitz, G.; Hajlaoui, M. E. *Adv. Mater.* **2000**, *12*, 1046.
(101) Chesterfield, R. J.; McKeen, J. C.; Newman, C. R.; Ewbank, P. C.; da Silva, D. A.; Bredas, J. L.; Miller, L. L.; Mann, K. R.; Frisbie, C. D. *J. Phys. Chem. B* **2004**, *108*, 19281.
(102) Nikitenko, V. R.; Heil, H.; von Seggern, H. *J. Appl. Phys.* **2003**, *94*, 2480.
(103) Schein, L. B.; Mcghie, A. R. *Phys. Rev. B* **1979**, *20*, 1631.
(104) Goh, C.; Kline, R. J.; McGehee, M. D.; Kadnikova, E. N.; Frechet, J. M. J. *Appl. Phys. Lett.* **2005**, *86*, 122110.
(105) Zhu, W.; Singer, S. J.; Zheng, Z.; Conlisk, A. T. *Phys. Rev. E* **2005**, *71*, 041501.
(106) Mozer, A. J.; Denk, P.; Scharber, M. C.; Neugebauer, H.; Sariciftci, N. S. *J. Phys. Chem. B* **2004**, *108*, 5235.
(107) Gill, W. D. *J. Appl. Phys.* **1972**, *43*, 5033.
(108) Pai, D. M. *J. Chem. Phys.* **1970**, *52*, 2285.
(109) Mozer, A. J.; Sariciftci, N. S.; Pivrikas, A.; Osterbacka, R.; Juska, G.; Brassat, L.; Bassler, H. *Phys. Rev. B* **2005**, *71*, 035214.
(110) Mozer, A. J.; Sariciftci, N. S. *Chem. Phys. Lett.* **2004**, *389*, 438.
(111) Zen, A.; Pflaum, J.; Hirschmann, S.; Zhuang, W.; Jaiser, F.; Asawapirom, U.; Rabe, J. P.; Scherf, U.; Neher, D. *Adv. Funct. Mater.* **2004**, *14*, 757.
(112) Rang, Z.; Haraldsson, A.; Kim, D. M.; Ruden, P. P.; Nathan, M. I.; Chesterfield, R. J.; Frisbie, C. D. *Appl. Phys. Lett.* **2001**, *79*, 2731.
(113) Chandrasekhar, M.; Guha, S.; Graupner, W. *Adv. Mater.* **2001**, *13*, 613.
(114) Liu, C. Y.; Bard, A. J. *Nature* **2002**, *418*, 162.
(115) Pasveer, W. F.; Cottaar, J.; Tanase, C.; Coehoorn, R.; Bobbert, P. A.; Blom, P. W. M.; de Leeuw, D. M.; Michels, M. A. J. *Phys. Rev. Lett.* **2005**, *94*, 206601.
(116) Lemaur, V.; Da Silva Filho, D. A.; Coropceanu, V.; Lehmann, M.; Geerts, Y.; Piris, J.; Debije, M. G.; Van de Craats, A. M.; Senthilkumar, K.; Siebbeles, L. D. A.; Warman, J. M.; Bredas, J. L.; Cornil, J. *J. Am. Chem. Soc.* **2004**, *126*, 3271.
(117) Silinsh, E.; Cápek, V. *Organic Molecular Crystals: Interaction, Localization, and Transport Phenomena*; American Institute of Physics: New York, 1994.
(118) Della Valle, R. G.; Venuti, E.; Farina, L.; Brillante, A.; Masino, M.; Girlando, A. *J. Phys. Chem. B* **2004**, *108*, 1822.
(119) Tiago, M. L.; Northrup, J. E.; Louie, S. G. *Phys. Rev. B* **2003**, *67*, 115212.
(120) Troisi, A.; Orlandi, G. *J. Phys. Chem. B* **2005**, *109*, 1849.
(121) Troisi, A.; Orlandi, G.; Anthony, J. E. *Chem. Mater.* **2005**, *17*, 5024.
(122) Hutchison, G. R.; Ratner, M. A.; Marks, T. J. *J. Am. Chem. Soc.* **2005**, *127*, 16866.
(123) Kwon, O.; Coropceanu, V.; Gruhn, N. E.; Durivage, J. C.; Laquindanum, J. G.; Katz, H. E.; Cornil, J.; Bredas, J. L. *J. Chem. Phys.* **2004**, *120*, 8186.
(124) Knipp, D.; Street, R. A.; Volkel, A.; Ho, J. *J. Appl. Phys.* **2003**, *93*, 347.
(125) Holstein, T. *Ann. Phys.* **1959**, *8*, 325.
(126) Holstein, T. *Ann. Phys.* **1959**, *8*, 343.
(127) Munn, R. W.; Silbey, R. *J. Chem. Phys.* **1985**, *83*, 1843.
(128) Munn, R. W.; Silbey, R. *J. Chem. Phys.* **1985**, *83*, 1854.
(129) Zhao, Y.; Brown, D. W.; Lindenberg, K. *J. Chem. Phys.* **1994**, *100*, 2335.
(130) Hannewald, K.; Stojanovic, V. M.; Bobbert, P. A. *J. Phys.: Condens. Matter* **2004**, *16*, 2023.
(131) Hannewald, K.; Stojanovic, V. M.; Schellekens, J. M. T.; Bobbert, P. A.; Kresse, G.; Hafner, J. *Phys. Rev. B* **2004**, *69*, 075211.
(132) Stojanovic, V. M.; Bobbert, P. A.; Michels, M. A. J. *Phys. Rev. B* **2004**, *69*, 144302.
(133) Peierls, R. E. *Quantum Theory of Solids*; Clarendon Press: Oxford, 1955.
(134) Conwell, E. M. *Phys. Rev. B* **1980**, *22*, 1761.
(135) Kittel, C. *Quantum Theory of Solids*; Rev. printing. ed.; Wiley: New York, 1963.
(136) Brüesch, P. *Phonons, Theory and Experiments*; Springer-Verlag: Berlin; New York, 1982.
(137) Newton, M. D. *Chem. Rev.* **1991**, *91*, 767.
(138) Balzani, V. *Electron Transfer in Chemistry*; Wiley-VCH: Weinheim; New York, 2001.
(139) Demadis, K. D.; Hartshorn, C. M.; Meyer, T. J. *Chem. Rev.* **2001**, *101*, 2655.
(140) *Electron Transfer from Isolated Molecules to Biomolecules*; Jortner, J.; Bixon, M., Eds.; Wiley: New York, 1999.
(141) Marcus, R. A. *Rev. Mod. Phys.* **1993**, *65*, 599.
(142) Cave, R. J.; Newton, M. D. *Chem. Phys. Lett.* **1996**, *249*, 15.
(143) Creutz, C.; Newton, M. D.; Sutin, N. *J. Photochem. Photobiol., A* **1994**, *82*, 47.
(144) Brunschwig, B. S.; Creutz, C.; Sutin, N. *Chem. Soc. Rev.* **2002**, *31*, 168.
(145) Hush, N. S. *Coord. Chem. Rev.* **1985**, *64*, 135.
(146) Barbara, P. F.; Meyer, T. J.; Ratner, M. A. *J. Phys. Chem.* **1996**, *100*, 13148.
(147) Hush, N. S. *Prog. Inorg. Chem.* **1967**, *8*, 391.
(148) Mikkelsen, K. V.; Ratner, M. A. *Chem. Rev.* **1987**, *87*, 113.
(149) Naleway, C. A.; Curtiss, L. A.; Miller, J. R. *J. Phys. Chem.* **1991**, *95*, 8434.
(150) Huang, J. S.; Kertesz, M. *Chem. Phys. Lett.* **2004**, *390*, 110.
(151) Cornil, J.; Calbert, J. P.; Bredas, J. L. *J. Am. Chem. Soc.* **2001**, *123*, 1250.
(152) Cheng, Y. C.; Silbey, R. J.; da Silva, D. A.; Calbert, J. P.; Cornil, J.; Bredas, J. L. *J. Chem. Phys.* **2003**, *118*, 3764.
(153) da Silva, D. A.; Kim, E. G.; Bredas, J. L. *Adv. Mater.* **2005**, *17*, 1072.
(154) Jordan, K. D.; Paddonrow, M. N. *J. Phys. Chem.* **1992**, *96*, 1188.
(155) Paddon-Row, M. N.; Jordan, K. D. *J. Am. Chem. Soc.* **1993**, *115*, 2952.
(156) Liang, C. X.; Newton, M. D. *J. Phys. Chem.* **1992**, *96*, 2855.
(157) Pati, R.; Karna, S. P. *J. Chem. Phys.* **2001**, *115*, 1703.
(158) Troisi, A.; Orlandi, G. *J. Phys. Chem. A* **2006**, *110*, 4065.
(159) Lu, S. Z.; Li, X. Y.; Liu, J. F. *J. Phys. Chem. A* **2004**, *108*, 4125.
(160) Koopmans, T. *Physica* **1934**, *1*, 104.
(161) RodriguezMonge, L.; Larsson, S. *J. Phys. Chem.* **1996**, *100*, 6298.
(162) Blancafort, L.; Voityuk, A. A. *J. Phys. Chem. A* **2006**, *110*, 6426.
(163) Senthilkumar, K.; Grozema, F. C.; Bickelhaupt, F. M.; Siebbeles, L. D. A. *J. Chem. Phys.* **2003**, *119*, 9809.
(164) Lowdin, P. O. *J. Chem. Phys.* **1950**, *18*, 365.
(165) Huang, J. S.; Kertesz, M. *J. Chem. Phys.* **2005**, *122*, 234707.
(166) Pietro, W. J.; Marks, T. J.; Ratner, M. A. *J. Am. Chem. Soc.* **1985**, *107*, 5387.
(167) Binstead, R. A.; Reimers, J. R.; Hush, N. S. *Chem. Phys. Lett.* **2003**, *378*, 654.
(168) Koch, N.; Vollmer, A.; Salzmann, I.; Nickel, B.; Weiss, H.; Rabe, J. P. *Phys. Rev. Lett.* **2006**, *96*, 156803.
(169) Coropceanu, V.; Nakano, T.; Gruhn, N. E.; Kwon, O.; Yade, T.; Katsukawa, K.; Bredas, J. L. *J. Phys. Chem. B* **2006**, *110*, 9482.
(170) Hummer, K.; Ambrosch-Draxl, C. *Phys. Rev. B* **2005**, *72*, 205205.
(171) de Wijs, G. A.; Mattheus, C. C.; de Groot, R. A.; Palstra, T. T. M. *Synth. Met.* **2003**, *139*, 109.
(172) Ferretti, A.; Ruini, A.; Bussi, G.; Molinari, E.; Caldas, M. J. *Phys. Rev. B* **2004**, *69*, 205205.
(173) Doi, K.; Yoshida, K.; Nakano, H.; Tachibana, A.; Tanabe, T.; Kojima, Y.; Okazaki, K. *J. Appl. Phys.* **2005**, *98*, 113709.

(174) Ponomarev, V. I.; Filipenko, O. S.; Atovmyan, L. O. *Kristallografiya* **1976**, *21*, 392.

(175) Brock, C. P.; Dunitz, J. D. *Acta Crystallogr., Sect. B: Struct. Sci.* **1990**, *46*, 795.

(176) Bulgarovskaya, I.; Vozzhennikov, V.; Aleksandrov, S.; Belskii, V. *Latv. PSR Zinat. Akad. Vestis, Fiz. Teh. Zinat. Ser.* **1983**, 53.

(177) Kearley, G. J.; Johnson, M. R.; Tomkinson, J. *J. Chem. Phys.* **2006**, *124*, 044514.

(178) Hermet, P.; Bantignies, J. L.; Rahmani, A.; Sauvajol, J. L.; Johnson, M. R. *J. Phys.: Condens. Matter* **2004**, *16*, 7385.

(179) Hermet, P.; Bantignies, J. L.; Rahmani, A.; Sauvajol, J. L.; Johnson, M. R. *J. Phys. Chem. A* **2005**, *109*, 4202.

(180) Hermet, P.; Bantignies, J. L.; Rahmani, A.; Sauvajol, J. L.; Johnson, M. R.; Serein, F. *J. Phys. Chem. A* **2005**, *109*, 1684.

(181) van Eijck, L.; Johnson, M. R.; Kearley, G. J. *J. Phys. Chem. A* **2003**, *107*, 8980.

(182) Plazanet, M.; Beraud, A.; Johnson, M.; Krisch, M.; Trommsdorff, H. P. *Chem. Phys.* **2005**, *317*, 153.

(183) Johnson, M. R.; Trommsdorff, H. P. *Chem. Phys. Lett.* **2002**, *364*, 34.

(184) Day, G. M.; Price, S. L.; Leslie, M. *J. Phys. Chem. B* **2003**, *107*, 10919.

(185) Gray, A. E.; Day, G. M.; Leslie, M.; Price, S. L. *Mol. Phys.* **2004**, *102*, 1067.

(186) Brillante, A.; Bilotti, I.; Della Valle, R. G.; Venuti, E.; Masino, M.; Girlando, A. *Adv. Mater.* **2005**, *17*, 2549.

(187) Masino, M.; Girlando, A.; Brillante, A.; Farina, L.; Della Valle, R. G.; Venuti, E. *Macromol. Symp.* **2004**, *212*, 375.

(188) Brillante, A.; Della Valle, R. G.; Farina, L.; Girlando, A.; Masino, M.; Venuti, E. *Chem. Phys. Lett.* **2002**, *357*, 32.

(189) Venuti, E.; Della Valle, R. G.; Brillante, A.; Masino, M.; Girlando, A. *J. Am. Chem. Soc.* **2002**, *124*, 2128.

(190) Girlando, A.; Masino, M.; Visentini, G.; Della Valle, R. G.; Brillante, A.; Venuti, E. *Phys. Rev. B* **2000**, *62*, 14476.

(191) Girlando, A.; Masino, M.; Visentini, G.; Brillante, A.; Della Valle, R. G.; Venuti, E. *Synth. Met.* **2000**, *109*, 13.

(192) Munn, R. W.; Siebrand, W. *J. Chem. Phys.* **1970**, *52*, 6391.

(193) Gruhn, N. E.; da Silva, D. A.; Bill, T. G.; Malagoli, M.; Coropceanu, V.; Kahn, A.; Bredas, J. L. *J. Am. Chem. Soc.* **2002**, *124*, 7918.

(194) Coropceanu, V.; Malagoli, M.; da Silva, D. A.; Gruhn, N. E.; Bill, T. G.; Bredas, J. L. *Phys. Rev. Lett.* **2002**, *89*, 275503.

(195) Kato, T.; Yamabe, T. *J. Chem. Phys.* **2001**, *115*, 8592.

(196) Kato, T.; Yamabe, T. *J. Chem. Phys.* **2003**, *119*, 11318.

(197) Kato, T.; Yoshizawa, K.; Yamabe, T. *Chem. Phys. Lett.* **2001**, *345*, 125.

(198) Coropceanu, V.; Kwon, O.; Wex, B.; Kaafarani, B. R.; Gruhn, N. E.; Durivage, J. C.; Neckers, D. C.; Bredas, J. L. *Chem. Eur. J.* **2006**, *12*, 2073.

(199) Malagoli, M.; Coropceanu, V.; da Silva, D. A.; Bredas, J. L. *J. Chem. Phys.* **2004**, *120*, 7490.

(200) Sanchez-Carrera, R. S.; Coropceanu, V.; da Silva, D. A.; Friedlein, R.; Osikowicz, W.; Murdey, R.; Suess, C.; Salaneck, W. R.; Bredas, J. L. *J. Phys. Chem. B* **2006**, *110*, 18904.

(201) da Silva, D. A.; Friedlein, R.; Coropceanu, V.; Ohrwall, G.; Osikowicz, W.; Suess, C.; Sorensen, S. L.; Svensson, S.; Salaneck, W. R.; Bredas, J. L. *Chem. Commun.* **2004**, 1702.

(202) Coropceanu, V.; Andre, J. M.; Malagoli, M.; Bredas, J. L. *Theor. Chem. Acc.* **2003**, *110*, 59.

(203) da Silva Filho, D. A.; Coropceanu, V.; Fichou, D.; Gruhn, N. E.; Bill, T. G.; Gierschner, J.; Cornil, J.; Brédas, J. L. *Philos. Trans. R. Soc. London, A* **2007**, accepted.

(204) Efrima, S.; Metiu, H. *Chem. Phys. Lett.* **1979**, *60*, 226.

(205) Gosar, P.; Choi, S. I. *Phys. Rev.* **1966**, *150*, 529.

(206) Vilfan, I. *Phys. Status Solidi B* **1973**, *59*, 351.

(207) Gosar, P.; Vilfan, I. *Mol. Phys.* **1970**, *18*, 49.

(208) Friedman, L. *Solid State Commun.* **1981**, *40*, 41.

(209) Casian, A.; Dusciac, V.; Coropceanu, I. *Phys. Rev. B* **2002**, *66*, 165404.

(210) Brovchenko, I. V. *Chem. Phys. Lett.* **1997**, *278*, 355.

(211) Friedman, L. *Phys. Rev.* **1965**, *140*, 1649.

(212) Deng, W. Q.; Goddard, W. A. *J. Phys. Chem. B* **2004**, *108*, 8614.

(213) Sinova, J.; Schliemann, J.; Nunez, A. S.; MacDonald, A. H. *Phys. Rev. Lett.* **2001**, *87*, 226802.

(214) Della Valle, R. G.; Brillante, A.; Farina, L.; Venuti, E.; Masino, M.; Girlando, A. *Mol. Cryst. Liq. Cryst.* **2004**, *416*, 145.

(215) Pedron, D.; Speghini, A.; Mulloni, V.; Bozio, R. *J. Chem. Phys.* **1995**, *103*, 2795.

(216) Eley, D. D. *Nature* **1948**, *162*, 819.

(217) Akamatsu, H.; Inokuchi, H. *J. Chem. Phys.* **1952**, *20*, 1481.

(218) Akamatsu, H.; Inokuchi, H. *J. Chem. Phys.* **1950**, *18*, 810.

(219) Inokuchi, H.; Harada, Y. *Nature* **1963**, *198*, 477.

(220) Kallmann, H. P.; Pope, M. *J. Chem. Phys.* **1960**, *32*, 300.

(221) LeBlanc, O. H., Jr. *J. Chem. Phys.* **1961**, *35*, 1275.

(222) Kepler, R. G. *Phys. Rev. Lett.* **1967**, *18*, 951.

(223) Kepler, R. G.; Bierstedt, P. E.; Merrifield, R. E. *Phys. Rev. Lett.* **1960**, *5*, 503.

(224) Pope, M.; Magnante, P.; Kallmann, H. P. *J. Chem. Phys.* **1963**, *38*, 2042.

(225) Helfrich, W.; Schneider, W. G. *Phys. Rev. Lett.* **1965**, *14*, 229.

(226) Katz, J. I.; Jortner, J.; Choi, S.; Rice, S. A. *J. Chem. Phys.* **1963**, *39*, 1683.

(227) Silbey, R.; Jortner, J.; Rice, S. A.; Vala, M. T. *J. Chem. Phys.* **1965**, *42*, 733.

(228) Silbey, R.; Munn, R. W. *J. Chem. Phys.* **1980**, *72*, 2763.

(229) Berry, R. S.; Jortner, J.; Mackie, J. C.; Pysh, E. S.; Rice, S. A. *J. Chem. Phys.* **1965**, *42*, 1535.

(230) Burland, D. M. *Phys. Rev. Lett.* **1974**, *33*, 833.

(231) Chance, R. R.; Braun, C. L. *J. Chem. Phys.* **1973**, *59*, 2269.

(232) Chance, R. R.; Braun, C. L. *J. Chem. Phys.* **1976**, *64*, 3573.

(233) Karl, N.; Stehle, R.; Warta, W. *Mol. Cryst. Liq. Cryst.* **1985**, *120*, 247.

(234) Warta, W.; Stehle, R.; Karl, N. *Appl. Phys. a-Mater. Sci. Process.* **1985**, *36*, 163.

(235) Schein, L. B. *Chem. Phys. Lett.* **1977**, *48*, 571.

(236) Schein, L. B.; Duke, C. B.; Mcghie, A. R. *Phys. Rev. Lett.* **1978**, *40*, 197.

(237) Schein, L. B.; Warta, W.; Mcghie, A. R.; Karl, N. *Chem. Phys. Lett.* **1983**, *100*, 34.

(238) Schein, L. B.; Narang, R. S.; Anderson, R. W.; Meyer, K. E.; Mcghie, A. R. *Chem. Phys. Lett.* **1983**, *100*, 37.

(239) Braun, C. L.; Scott, T. W. *J. Phys. Chem.* **1983**, *87*, 4776.

(240) Parris, R. E.; Kenkre, V. M.; Dunlap, D. H. *Phys. Rev. Lett.* **2001**, *8712*.

(241) Parris, P. E.; Dunlap, D. H.; Kenkre, V. M. *Phys. Status Solidi B-Basic Res.* **2000**, *218*, 47.

(242) Kenkre, V. M.; Andersen, J. D.; Dunlap, D. H.; Duke, C. B. *Phys. Rev. Lett.* **1989**, *62*, 1165.

(243) Kenkre, V. M.; Dunlap, D. H. *Philos. Mag. B* **1992**, *65*, 831.

(244) Scher, H.; Montroll, E. W. *Phys. Rev. B* **1975**, *12*, 2455.

(245) Bassler, H.; Schonherr, G.; Abkowitz, M.; Pai, D. M. *Phys. Rev. B* **1982**, *26*, 3105.

(246) Bassler, H. *Philos. Mag. B* **1984**, *50*, 347.

(247) Silver, M.; Schoenherr, G.; Baessler, H. *Phys. Rev. Lett.* **1982**, *48*, 352.

(248) Haarer, D. *Festkoerperprobleme* **1990**, *30*, 157.

(249) Haarer, D. *Angew. Makromol. Chem.* **1990**, *183*, 197.

(250) *Physics and Chemistry of the Organic Solid State*; Fox, D.; Labes, M. M.; Weissberger, A., Eds.; Interscience Publishers: New York, 1963−1967; Vol. I−III.

(251) Böttger, H.; Bryksin, V. V. *Hopping Conduction in Solids*; VCH: Deerfield Beach, FL, 1985.

(252) Emin, D. *Adv. Phys.* **1975**, *24*, 305.

(253) Klinger, M. I.; Sykes, J. B. *Problems of Linear Electron (Polaron) Transport Theory in Semiconductors*, 1st ed.; Pergamon Press: Oxford; New York, 1979.

(254) Movaghar, B. *J. Mol. Electron.* **1987**, *3*, 183.

(255) Glaeser, R. M.; Berry, R. S. *J. Chem. Phys.* **1966**, *44*, 3797.

(256) Fratini, S.; Ciuchi, S. *Phys. Rev. Lett.* **2003**, *91*, 256403.

(257) Friedman, L. *Phys. Rev. A* **1964**, *135*, A233.

(258) Nitzan, A.; Mukamel, S.; Jortner, J. *J. Chem. Phys.* **1975**, *63*, 200.

(259) Appel, J. In *Solid State Physics*; Seitz, F., Turnbull, D., Ehrenreich, H., Eds.; Academic Press: New York, 1968; Vol. 21, 193.

(260) Hannewald, K.; Bobbert, P. A. *Appl. Phys. Lett.* **2004**, *85*, 1535.

(261) Hultell, M.; Stafstrom, S. *Chem. Phys. Lett.* **2006**, *428*, 446.

(262) Troisi, A.; Orlandi, G. *Phys. Rev. Lett.* **2006**, *96*, 086601.

(263) Miller, A.; Abrahams, E. *Phys. Rev.* **1960**, *120*, 745.

(264) Olivier, Y.; Lemaur, V.; Bredas, J. L.; Cornil, J. *J. Phys. Chem. A* **2006**, *110*, 6356.

(265) Arkhipov, V. I.; Fishchuk, I. I.; Kadashchuk, A.; Baessler, H. *Photophys. Mol. Mater.* **2006**, 261.

(266) Yu, Z. G.; Smith, D. L.; Saxena, A.; Martin, R. L.; Bishop, A. R. *Phys. Rev. B* **2001**, *6308*, 085202.

(267) Yu, Z. G.; Smith, D. L.; Saxena, A.; Martin, R. L.; Bishop, A. R. *Phys. Rev. Lett.* **2000**, *84*, 721.

(268) Rakhmanova, S. V.; Conwell, E. M. *Synth. Met.* **2001**, *116*, 389.

(269) Gartstein, Y. N.; Conwell, E. M. *Chem. Phys. Lett.* **1995**, *245*, 351.

(270) Coehoorn, R.; Pasveer, W. F.; Bobbert, P. A.; Michels, M. A. J. *Phys. Rev. B* **2005**, *72*, 155206.